

学校代码	10699
分类号	V421.1
密 级	
学 号	2018280050

题目 Design and Control for Reusable
Booster of Launch Vehicle

作者 Simon LE BERRE

学科、专业 飞行器设计

指导教师 龚春林

申请学位日期 2020 年 5 月

西北工业大学
硕士学位论文
(学位研究生)

题目: Design and Control for Reusable
Booster of Launch Vehicle

作者: SIMON LE BERRE
学科专业: 飞行器设计
指导教师: 龚春林

2020 年 5 月

**Title: Design and Control for Reusable Booster of Launch
Vehicle**

By
SIMON LE BERRE

Under the Supervision of Professor
GONG CHUNLION

A Dissertation Submitted to
Northwestern Polytechnical University

In partial fulfillment of the requirement
For the degree of
Master of Flight Vehicle Design

Xi'an P. R. China
May 2020

Abstract

Scientists tell us the human who will walk on Mars's surface was already born. Fact to understand space conquest is entering a new golden age. This time, national agencies such as NASA are not playing alone the leading role; some private companies are also extremely ambitious.

With the evolution of the propulsion engines, and thanks to new liquid engine nearly as powerful as a solid one, and controlling the engine restart as well as an aircraft engine, the challenge to control the atmosphere reentry of Launch Vehicle has become a reality. This time the booster will come back to the Earth and can be overhauled and ready to work again and again. These boosters have for the moment one main mission: satellite orbiting. The next application for the boosters is to build a RLV for the human exploration of the Moon or Mars. Another usage would be to create the fastest human transport to link two points of our planet using orbital speed. To realize all these very ambitious projects one problem remains: How to use the atmosphere to come back to the Earth? To answer this question, this thesis has been divided into four parts.

Firstly, this research proposes a revision of the shape of the RLV, by simulating the airflow. Beginning with the examination of an additional flight controller to an overall review of the shape, simulation and aerospace requirements have led to the selection of the best trajectory controller rather than the best drag system.

Secondly, based on these results, the impact of the trajectory controller has been studied. The goal was to improve the trajectory to optimize the aerodynamic properties of the RLV. It has been demonstrated that it was possible to achieve an almost vertical reentry while having a high drag force.

Thirdly, the final step of landing is to control the balance during the last few meters before landing. When the speed is low, therefore the aerodynamic effects are negligible. The non-linear problem is close to a three-dimensional inverted pendulum with altitude control. It has been modeled with MATLAB/Simulink and controlled by a double nested PID loop for horizontal translation, coupled with one PID loop for the altitude.

In the last part, to put all the theoretical and simulation results into perspectives, and to cope with the design problems known to aerospace companies, real RLV models have been

designed, built, and tested. Thanks to the experience gained during the construction, and the programming of the first models, the last one is optimized and works like a real vector rocket.

Keywords: reusable launch vehicle, air brakes, air controller, trajectory controller, PID control, vector rocket.

Table of contents

Abstract	IV
Acronymes	IX
List of tables	IX
List of figures	XI
Chapter 1 Introduction	15
1.1 Background	15
1.2 Relative works.....	17
1.2.2 RLV Trajectory optimization	18
1.2.3 Vector rocket stabilization.....	18
1.2.4 Model of RLV work.....	19
1.3 Objective and contents	19
Chapter 2 Improvement RLV shape design	20
2.1 RLV Baseline Description.....	20
2.2 Validation of process	20
2.3.1. Solidworks model	21
2.3.2. Drag force definition.....	21
2.3.3. Reynold number definition	21
2.3.4. Flow simulation	21
2.3.5. Validation of test.....	23
2.3 Falcon 9's grid fin	23
2.3.2. Grid fins idea	23
2.3.3. Falcon 9's structure.....	24
2.4 Trajectory controllers	26
2.4.1. Comparison.....	26
2.4.2. Possible improvement.....	26
2.4.3. Grid fin	27
2.4.4. Flat fin	28
2.4.5. Bell brake.....	29
2.4.6. Simple fin	30
2.4.7. Strength of materials.....	31
2.4.8. Results and comparison	32

TABLE OF CONTENT

2.4.9.	Final model.....	35
2.5	Global review of RLV shape	35
2.5.1	Top shape of RLV	35
2.5.2	Air to Air brake.....	36
2.6	Rotary idea to keep RLV balance	38
2.6.1	Personal idea.....	38
2.6.2	Other ways to use rotary recovery system	40
2.7	Conclusion	41
Chapter 3 Trajectory design and simulation		42
3.1	Introduction	42
3.2	Background and Objectives	43
3.3	Equation of trajectory control.....	43
3.4	Air density function of altitude	45
3.5	Aerodynamic forces	46
3.6	Velocity line and temperature visualization	51
3.7	MATLAB Simulink model.....	53
3.7.1	Presentation	53
3.7.2	Result	55
3.8	Conclusion	64
Chapter 4 End phase control design.....		65
4.1	Introduction	65
4.2	Inversed pendulum model	66
4.3	3-dimensional model.....	68
4.4	PID control.....	68
4.4.1	Presentation	68
4.4.2	PID curves control	70
4.4.3	Equation of PID coefficient	71
4.5	Altitude control	71
4.5.1	Presentation	71
4.5.2	MATLAB Simulink model	72
4.6	Control parameter.....	73
4.7	Global MATLAB Simulink.....	74
4.8	3D Virtual world.....	74
4.9	Result of simulation	75

TABLE OF CONTENT

4.10 Conclusion	76
Chapter 5 Validation of end phase control.....	78
5.1 Introduction	78
5.2 Origns of the idea to build a vector rocket?	79
5.3 Characteristic of the model	79
5.4 RLV Model 1	80
5.5 RLV Model 2.....	81
5.6 RLV Model 3.....	82
5.7 RLV Model 4.....	83
5.8 Analysis and remarks	84
5.8.1 3D printing.....	84
5.8.2 Programming control	84
5.9 Special device developed	84
5.9.1 Vision system.....	84
5.9.2 Support of Flight control system	86
5.10 Conclusion	86
Chapter 6 Conclusion.....	87
6.1 Summary	87
6.2 Discussion and future works	87
Bibliography.....	89
Annexe	91

Acronyms

LV	Lauch Vehicle
RLV	Reusable Lauch Vehicle
ISS	International Space Station
ESA	European space Agency
NASA	National Aeronautics and Space Administration
PID	Proportional, integrator and derivate
PD	Proportional and derivate
Re	Reynold number
2D	Tow dimensions
3D	Three dimensions
PLA	PloyLactic Acid
FC	Flight Controller
ESC	Electronic Speed Controller
EDF	Electro Ducted Fan
UAV	Unmanned Aircraft Systems

ACRONYMES

List of tables

<i>Table 2.1 Drag force test of sphere function of Reynolds number</i>	<i>Page 6</i>
<i>Table 2.2 Forces generated by the Grid fin</i>	<i>Page 12</i>
<i>Table 2.3 Force generated by the Flat fin</i>	<i>Page 13</i>
<i>Table 2.4 Forces generated by the Bell brake</i>	<i>Page 14</i>
<i>Table 2.5 Forces generated by the Simple fin</i>	<i>Page 15</i>
<i>Table 2.6 Drag force for every trajectory controller</i>	<i>Page 16</i>
<i>Table 2.7 Lift force of every trajectory controller</i>	<i>Page 17</i>
<i>Table 3.1 Force applied on the RLV function of the attack angle</i>	<i>Page 27</i>
<i>Table 3.2 Force applied on the RLV and ratio function of the attack angle</i>	<i>Page 28</i>
<i>Table 4.1 PID explication</i>	<i>Page 49</i>

LIST OF TABLES

List of figures

<i>Figure 1.1 Representation of all satellites around the Earth</i>	<i>Page 1</i>
<i>Figure 1.2 Two Falcon 9's boosters from the Falcon</i>	<i>Page 2</i>
<i>Figure 1.3 The Space X Project Starship during the take-off phase</i>	<i>Page 2</i>
<i>Figure 1.4 Space Shuttle Atlantis STS-129 during the landing phase</i>	<i>Page 3</i>
<i>Figure 1.5 The RLV from Blue Origin named "New Shepard"</i>	<i>Page 4</i>
<i>Figure 2.1 Sphere inside air flux</i>	<i>Page 5</i>
<i>Figure 2.2 Representation of drag of sphere</i>	<i>Page 5</i>
<i>Figure 2.3 Graphic of Sphere drag coefficient function of Reynolds number</i>	<i>Page 6</i>
<i>Figure 2.4 Grid fins on soviet missiles, Military History Museum of Artillery</i>	<i>Page 8</i>
<i>Figure 2.5 Space X grid fins during assembly, Texas</i>	<i>Page 8</i>
<i>Figure 2.6 Three using of Space X's Grid fins on Falcon 9</i>	<i>Page 9</i>
<i>Figure 2.7 Real and model of Space X Falcon 9 booster</i>	<i>Page 9</i>
<i>Figure 2.8 Space X grid fins, 3D model</i>	<i>Page 11</i>
<i>Figure 2.9 Flow simulation: Air flux around Grid fin with 30° of control</i>	<i>Page 11</i>
<i>Figure 2.10 Flat fin, 3D model</i>	<i>Page 12</i>
<i>Figure 2.11 Flow simulation: Air flux around Flat fin with 30° of control</i>	<i>Page 12</i>
<i>Figure 2.12 Bell brake, 3D model</i>	<i>Page 13</i>
<i>Figure 2.13 Flow simulation: Air flux around Bell brake with 30° of control</i>	<i>Page 13</i>
<i>Figure 2.14 Simple fin, 3D model</i>	<i>Page 14</i>
<i>Figure 2.15 Flow simulation: Air flux around Simple fin with 30° of control</i>	<i>Page 14</i>
<i>Figure 2.16 Simulation of effort applied by air on the Flat fin</i>	<i>Page 15</i>
<i>Figure 2.17 Simulation of effort apply by air on the Bell brake</i>	<i>Page 16</i>
<i>Figure 2.18 Graph of drag forces generated by every trajectory controller</i>	<i>Page 17</i>
<i>Figure 2.19 Graph of lift force generated by every trajectory controller</i>	<i>Page 18</i>
<i>Figure 2.20 Simple fin on the RLV</i>	<i>Page 18</i>
<i>Figure 2.21 Fins assembled on the Space X Starship</i>	<i>Page 18</i>
<i>Figure 2.22 Different king of shape for the top of RLV with Value of drag force</i>	<i>Page 19</i>
<i>Figure 2.23 Air to Air Structure</i>	<i>Page 20</i>
<i>Figure 2.24 Mechanism of elbow</i>	<i>Page 20</i>
<i>Figure 2.25 Air flow trhough of the structure</i>	<i>Page 20</i>
<i>Figure 2.26 Flow simulation: Air flux around air to air structure</i>	<i>Page 20</i>
<i>Figure 2.27 Spinning top 3D model</i>	<i>Page 21</i>
<i>Figure 2.28 Water Spinning top and water pressure device</i>	<i>Page 21</i>

<i>Figure 2.29 Model of air flux rotation</i>	<i>Page 23</i>
<i>Figure 2.30 Parachute rotor blade system</i>	<i>Page 23</i>
<i>Figure 2.31 Rotary rocket</i>	<i>Page 24</i>
<i>Figure 2.32 Rotary parachute</i>	<i>Page 24</i>
<i>Figure 3.1 Graphic representation of the trajectory steps of the booster</i>	<i>Page 25</i>
<i>Figure 3.2 The re-entry burn of SpaceX Falcon 9's first stage</i>	<i>Page 26</i>
<i>Figure 3.3 Mechanical model of RLV during reentry phase</i>	<i>Page 27</i>
<i>Figure 3.4 Air density function of altitude (4000 m to sea level)</i>	<i>Page 29</i>
<i>Figure 3.5 Flow simulation model</i>	<i>Page 29</i>
<i>Figure 3.6 Force applied on the RLV function of the attack angle</i>	<i>Page 30</i>
<i>Figure 3.7 Drag and Lift force applied on the RLV function of the attack angle</i>	<i>Page 32</i>
<i>Figure 3.8 Ratio between drag force and drag force at 0°</i>	<i>Page 32</i>
<i>Figure 3.9 Ratio drag force and drag force at 0° between 0° and 25° (-)</i>	<i>Page 33</i>
<i>Figure 3.10 Ratio drag force and drag force at 0° between 25° (+) and 80°</i>	<i>Page 33</i>
<i>Figure 3.11 Ratio lift force and drag force between 0° and 30° (-).</i>	<i>Page 33</i>
<i>Figure 3.12 Ratio lift force and drag force between 30° (+) and 80°</i>	<i>Page 34</i>
<i>Figure 3.13 Velocity line for $\alpha=0^\circ$</i>	<i>Page 35</i>
<i>Figure 3.14 Velocity line for $\alpha = 20^\circ$</i>	<i>Page 35</i>
<i>Figure 3.15 Temperature wake for $\alpha = 0^\circ$</i>	<i>Page 35</i>
<i>Figure 3.16 Temperature wake for $\alpha = 20^\circ$</i>	<i>Page 35</i>
<i>Figure 3.17 Warmer point for $\alpha = 20^\circ$</i>	<i>Page 35</i>
<i>Figure 3.18 Mechanical model of RLV during reentry phase, force on x axis.</i>	<i>Page 36</i>
<i>Figure 3.19 Representation of attack angle</i>	<i>Page 37</i>
<i>Figure 3.20 Attack Angle 3D relation.</i>	<i>Page 38</i>
<i>Figure 3.21 Free fall without atmosphere.</i>	<i>Page 39</i>
<i>Figure 3.22 Free fall with atmosphere.</i>	<i>Page 40</i>
<i>Figure 3.23 Time Ratio curve function of angle attack.</i>	<i>Page 41</i>
<i>Figure 3.24 Reentry trajectory for 30° of attack angle.</i>	<i>Page 41</i>
<i>Figure 3.25 Angle attack for 30° of command.</i>	<i>Page 41</i>
<i>Figure 3.26 Reentry trajectory sinusoid command.</i>	<i>Page 42</i>
<i>Figure 3.27 Angle attack sinusoid command</i>	<i>Page 42</i>
<i>Figure 3.28 Reentry trajectory for small gate command</i>	<i>Page 43</i>
<i>Figure 3.29 Angle attack for small gate command.</i>	<i>Page 43</i>
<i>Figure 3.30 Reentry trajectory for large gate command.</i>	<i>Page 44</i>

<i>Figure 3.31 Angle attack for large gate command.</i>	<i>Page 44</i>
<i>Figure 3.32 Maple leaves trajectory.</i>	<i>Page 45</i>
<i>Figure 3.33 Reentry trajectory for 3D cercle command.</i>	<i>Page 45</i>
<i>Figure 3.34 Angle attack (pitch) for 3D cercle command.</i>	<i>Page 46</i>
<i>Figure 3.35 Angle attack (roll) for 3D cercle command.</i>	<i>Page 46</i>
<i>Figure 3.36 Graph of comparisons of the different trajectories design.</i>	<i>Page 47</i>
<i>Figure 3.37 Idea of RLV reentry trajecoty</i>	<i>Page 47</i>
<i>Figure 4.1 The two-lateral booster of the falcon heavy</i>	<i>Page 48</i>
<i>Figure 4.2 Graphic representation of the trajectory of the falcon 9</i>	<i>Page 49</i>
<i>Figure 4.3 RLV model system</i>	<i>Page 49</i>
<i>Figure 4.4 Coordinate system of engine force</i>	<i>Page 50</i>
<i>Figure 4.5 Equation of balance system from Newton laws</i>	<i>Page 51</i>
<i>Figure 4.6 From 2Dimensions systems to 3Dimensions</i>	<i>Page 51</i>
<i>Figure 4.7 Double loop PID, angle stability and position control</i>	<i>Page 51</i>
<i>Figure 4.8 PID blocks model</i>	<i>Page 52</i>
<i>Figure 4.9 Curve of PID coefficient function of length of RLV</i>	<i>Page 53</i>
<i>Figure 4.10 Double PID loop with angle PID autonomous control</i>	<i>Page 54</i>
<i>Figure 4.11 Simple loop PID altitude control</i>	<i>Page 55</i>
<i>Figure 4.12 Altitude of rocket subject to an altitude command + 10m and - 5m</i>	<i>Page 55</i>
<i>Figure 4.13 Altitude of rocket subject to many horizontal travels (fine scale)</i>	<i>Page 56</i>
<i>Figure 4.14 Angle value of real thrust of the engine</i>	<i>Page 56</i>
<i>Figure 4.15 Full Simulink model of vector rocket control (Annex 3.1)</i>	<i>Page 57</i>
<i>Figure 4.16 3D Virtual World</i>	<i>Page 57</i>
<i>Figure 4.17 RLV translation on 3D Virtual World</i>	<i>Page 58</i>
<i>Figure 4.18 Pitch and Roll of Engine</i>	<i>Page 58</i>
<i>Figure 4.19 Pitch and Roll of Body</i>	<i>Page 58</i>
<i>Figure 4.20 Pitch and Roll of Body</i>	<i>Page 59</i>
<i>Figure 4.21 XZ Graph trajectory of RLV</i>	<i>Page 59</i>
<i>Figure 4.22 Space X Starhopper during flight test in Texas</i>	<i>Page 60</i>
<i>Figure 5.1 Virtual view of RLV prototype</i>	<i>Page 61</i>
<i>Figure 5.2 Space X prototype Grasshopper reach 1000m in June 2013</i>	<i>Page 62</i>
<i>Figure 5.3 Virtual view of RLV Model 1</i>	<i>Page 63</i>
<i>Figure 5.4 Virtual view of RLV Model 2</i>	<i>Page 64</i>
<i>Figure 5.5 Virtual view of RLV Model 2</i>	<i>Page 65</i>

<i>Figure 5.6 Virtual view of RLV Model 4</i>	<i>Page 66</i>
<i>Figure 5.7 Solidworks view of vision system</i>	<i>Page 67</i>
<i>Figure 5.8 Solidworks view of vision system (bottom)</i>	<i>Page 67</i>
<i>Figure 5.12 Photo of the model print in 3D</i>	<i>Page 69</i>
<i>Figure 5.13 Photo of the flight controller inside the RLV Model 2 pipe</i>	<i>Page 69</i>

Chapter 1 Introduction

1.1 Background

How to use the atmosphere to come back to earth? No, this question does not excite me since I was 8 years old. However, many questions were in my mind since I was young. Most of the time they are not existential, but practical like how that works or how to improve it. Lately came this one: Why? It is a choice, motivated by my vision of the future. I think the Space become again at the center of all engineering challenges. With fast evolution of our society during these last decades, data and the internet connexion became essential. The demand for placing satellites in orbit has never been greater. As present the *Figure 1.1* human has already colonized the first layers of the space.



Figure 1.1 Representation of all satellites around the Earth

Since the first Russian satellite named "Sputnik" in 1957, mankind has put more than 8500 satellites into orbit. If the first satellites were intended for research and development, then for the military field with data transmission and later for geo-positioning such as GPS, GLONASS, Beidou, and Galileo. Today, a new era of satellites is beginning with the satellites that will provide the Internet to everyone all around the Earth. Many companies are present in this new market, so the demand for launches is constantly increasing. The possibility of reusing the engines or part of the structure will be of great help in lowering the price of access to orbit. Currently, only one company can lower the price of the launch by reusing the first stage. This is Space X with the Falcon 9 [1] and Falcon Heavy [2] launchers.



Figure 1.2 Two Falcon 9's boosters from the Falcon Heavy's first stage just before the touchdown

It is a great success and a new way for space exploration. The existing point is that this is only the beginning, with the mastery of these technologies, some of humanity's old dreams are now accessible and here what we failed 20 years ago seems accessible today. The project of colonizing another planet today makes sense. The exploration of Mars is planned for this decade and today, the engineers working on the design of the RLV will reach the Martian ground using the technologies developed for launch into orbit.

I expect within ten/twenty years successful research and development projects would lead to new types of “ground” transportation as well, meaning, not only for astronauts but also for people to reach each point of the earth within one hour thanks to the orbital speed [3,4].



Figure 1.3 The Space X Project Starship with his booster during the take-off phase

Before starting this thesis, it is necessary to clarify one point of vocabulary. The term RLV will be used for real RLV and for booster which can return to earth like the falcon 9 booster. Currently, two kinds of RLV have been built by human, the ones that are called “partial” and

the other ones that are “total”. The term partial concerns the RLV which need additional booster for the takeoff phase, most of the time solid one, like the Space shuttle [5].



Figure 1.4 Space Shuttle Atlantis STS-129 during the landing phase, November 27, 2009

The focus is on the landing phase so both kinds can be taken into account. However, the “total” RLV will be considered, so the ones with a shape close to a rocket and not to a plane.

Just a comment in that regard, note the interesting evolution of the RLV; if 30 years ago the idea was to use a plane shape, meaning with horizontal landing, today the vertical landing has been chosen. However, the idea used for the Space shuttle to reduce the speed is still valid to increase the drag force with attack angle of the RLV during this reentry phase.

1.2 Relative works

From reusable boosters to full RLV, projects are emerging all over the world. A quick overview of the most advanced international RLV projects is presented. European Space Agency (ESA) and the Ariane launchers [6,7] are lagging. However, some projects are in the design phase: this time it is RLV. The Callisto project [8] is for the medium term and the Themis project [9] for the long term. India, which was not an aerospace country, has entered the RLV race in recent years, and the main project is called RLV-TD [10], which is a two-stage project, the last one being an RLV, whose general shape is inspired by the Space Shuttle. China is also interested in the RLV and is in the race, LinkSpace's RLV-T5 [11] managed to reach 300 meters last summer, a promising first step. The giants of the market are American, helped by the huge financial contracts signed by the defense and NASA, some companies are growing so fast. As everyone knows, the leader today is Space X, which is the only one with experience and profits from the use of RLV. Other companies are actively participating in this development, such as Bleu Origin which is certainly the second largest in the world today. New Shepard [12] and New Glenn [13] are the main project from them in RLV.



Figure 1.5 The RLV from Blue Origin named “New Shepard” during the landing phase

For them, the development of RLV is not only for the cost saving of a satellite, but it is also a way to acquire the necessary technology for the next lunar journey with the Blue Moon project [14].

By choosing the RLV with a tube shape rather than a plane shape, the focus is on the trajectory controllers. Contrary to some devices present on the RLV which are very recent like the re-damping engines, the trajectory controller is a studied, known, and used technology. This use comes from missile engineering. However, some differences exist between the missile and the RLV. When the missile touches the ground with the nose and at its maximum speed, the RLV touches the ground from the bottom of the structure via a foot system and at a speed close to zero. Most of the fins used for missiles are of a very simple shape [15,16], just a tail. However, some studies have predicted that the missile could be controlled by a grid fin [17,18]. Regarding the trajectory controller used to control the re-entry phase of the RLV, some works are inspiring [19,20].

1.2.2 RLV Trajectory optimization

Since the achievement of the Apollo missions with the Space Shuttle, the scientific community has understood the economic interest of improving this atmospheric re-entry, it has also understood its complexity. Thus, while structurally it is complicated to determine the right compromise. It is the same for the trajectory, the first objective remains the safety of the structure and its landing without damage, but the second is to optimize the use of the drag force. For this, two lines of research exist: improving the engine use [21,22], and optimizing the angle of attack [23,24].

1.2.3 Vector rocket stabilization

This problem had been seen as a 3D inverted pendulum problem with altitude control. However, some considerations have been taken into account due to the control by thrust force

and engine angle and not by support translation. However, there are many commonalities between vector rocket control and 3D Reverse Pendulum control. To start the modeling, two relative works have been read [25,26].

1.2.4 Model of RLV work

Many companies with a small budget are trying to enter the launch vehicle market, especially since the development of the small satellite with low orbit, which makes the payload lighter and shorter distance shorter. However, for a student project, this is still quite impossible. The solution is therefore drone technology, whose parts are very inexpensive and which makes it possible to build very small rockets, less than a metre long. A few vector rockets projects [27,28] motivated the design of my model

1.3 Objective and contents

The objective of this research is to understand more about RLV engineering challenge. However, it is necessary to define the scope of the study: it starts after the loop maneuver in the case of booster, when the aerodynamic effects have to be taken account and ends just before landing. Thus, legs and landing device will not be studied.

Actually, two kinds of studies will be conducted. They are independent from each other.

- The first one, described in chapter 2 is the improvement of the RLV shape. Firstly, additional part as done by Space X with the grid fin. Secondly, some ideas of the global shape review of RLV will be proposed and reviewed.

- The best solution will be helpful for the second part of the study presented in chapter 3: Trajectory design and simulation. It is the control of the RLV during the atmospheric reentry. The aerodynamic effect function of the attack angle will be studied. Based on this result and input from the chapter 2, one design method of reentry will be presented.

- The chapter 4 will develop the last part of the reentry, just before the touch down. When the aerodynamic forces cannot control the verticality of the structure. The control is then entirely ensured by the motors. The problem is close to an inverted pendulum, however in this case it is a vector rocket moving in three dimensions.

- The last part of this thesis is the realization of an RLV model. For sure the size is much smaller than an RLV used by aerospace companies, however the challenge remains the same.

Chapter 2 Improvement RLV shape design

2.1 RLV Baseline Description

Since the beginning of the aerospace, many shapes of LV (Launch Vehicle) have been designed. However, the general aspect is close to the cylinder with one nose on the top and the propulsion on the bottom. RLV (Reusable Launch Vehicle) shapes can be very different, for example between the Space shuttle and booster of Falcon 9, the first one is close to a plane where the second is close to the shape of LV. The main difference is that the booster of Falcon 9 can take off without assistance; it is a booster. It is this case of RLV who will study and try to improve. Let's look at how Space X improved the traditional shape of LV to make it reusable. For this huge project Space X met many interesting challenges as the improvement of the propulsion and the development of Merlin Engine or the landing legs. Concerning the shape, engineers' SpaceX found the solution by improving an old technology; the grid fins [29]. In the beginning, the Space X grid fins will be studied. The future trajectory controller will be compared to the Space X one.

Given the huge size of the RLV, the only way to test the aerodynamic system is by computer modeling. The SolidWorks software is used to build a 3D model, then aerodynamic tests are computed via Flow simulation, a SolidWorks complement, to get the drag force value. However, the reliability of this process has to be tested. For that, one important problem has to be solved and compared: the drag coefficient of the sphere function of Reynold number [30]. Then, Space X's grid fin is created and tested; the aerodynamic characteristic of this one will be taken as reference and will be compared to other trajectory controllers.

Our study will analyze another part, very new in the aerospace conception which is to improve the inertia force [31] of the rocket by rotation, not the rotation of the RLV which would behave randomly but thanks to the air rotation.

The generic name of grid fins or any air barker chosen will be trajectory controller because the main objectives of these devices are primarily to controller the reentry trajectory and secondly to increase the drag force.

2.2 Validation of process

As explained in the introduction, the goal of this part is to validate process and software used. For that, a famous relation of aerodynamic: the drag coefficient of sphere function of Reynold number, will be studied. The result of the study will be compared to the graphic in *Figure 1.5* [32].

2.3.1. Solidworks model

Our model is a sphere placed on the constant air flux. Two variables are considered: the diameter of the sphere and the velocity of the flux.

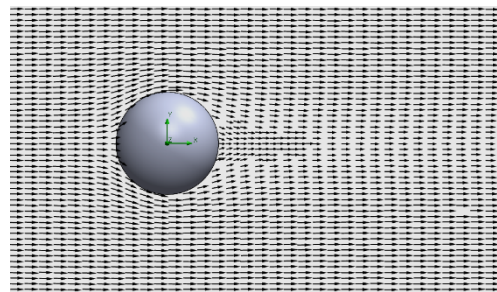


Figure 2.1 Sphere inside air flux

2.3.2. Drag force definition

$$F_d = \frac{1}{2} * C_D * V^2 * \rho_{air} * A \quad (2.1)$$

C_D : Drag coefficient

V: Velocity of the ball through the air

ρ_{air} : Air density = 1.225 kg/m³

A: Projected area = $\pi * r^2$

2.3.3. Reynold number definition

$$Re = \frac{\rho \cdot V \cdot L}{\mu} \quad (2.2)$$

ρ : Density of fluid

V: Speed of fluid

L: Linear dimension

μ : Dynamic viscosity of fluid

2.3.4. Flow simulation

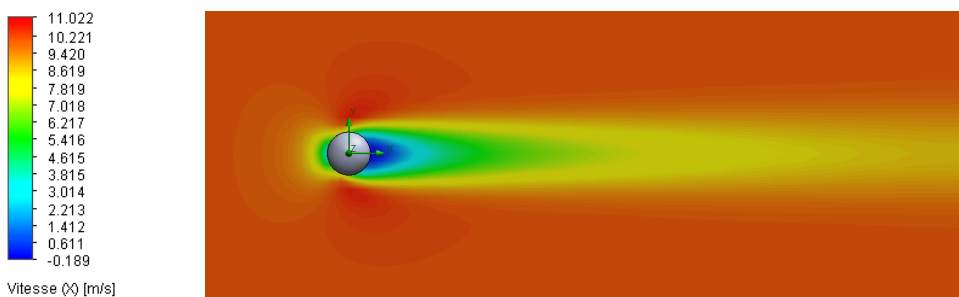


Figure 2.2 Representation of the sphere's drag

Calculation table:

Few series of tests have been conducted:

The first one is low random values of Re number.

The second one is low fixed values of Re number.

The third one is it with fixed diameter value.

The fourth one is it with fixed speed value.

The last one is high fixed values of Re number.

Table 2.1 Drag force test of sphere function of Reynolds number

Diameter (m)	Speed (m/s)	density of fluid	dynamic viscosity	Re	Cx
2,00E-04	6,04E-01	1,225	1,48E-05	1,00E+01	1,16
1,00E-03	3,62E+00	1,225	1,48E-05	3,00E+02	0,639
2,00E-03	1,09E+01	1,225	1,48E-05	1,80E+03	0,359
1,00E-02	1,09E+01	1,225	1,48E-05	9,00E+03	0,277
7,77E-02	2,00E+01	1,225	1,48E-05	1,00E+04	0,233
1,10E-01	1,00E+01	1,225	1,48E-05	1,00E+04	0,2396
1,55E-01	5,00E+00	1,225	1,48E-05	1,00E+04	0,241
3,48E-01	1,00E+00	1,225	1,48E-05	1,00E+04	0,2509
0,11	1,00E+00	1,225	1,48E-05	2,86E+04	0,2767
0,11	5,00E+00	1,225	1,48E-05	1,43E+05	0,2467
0,11	1,00E+01	1,225	1,48E-05	2,86E+05	0,2396
0,11	2,00E+01	1,225	1,48E-05	5,72E+05	0,2344
0,11	27,8	1,225	1,48E-05	7,95E+05	0,235
0,22	27,8	1,225	1,48E-05	1,59E+06	0,231
0,33	27,8	1,225	1,48E-05	2,39E+06	0,23
0,44	27,8	1,225	1,48E-05	3,18E+06	0,229
3,48E+00	100	1,225	1,48E-05	1,00E+08	0,249
4,92E+00	50	1,225	1,48E-05	1,00E+08	0,237
1,10E+01	10	1,225	1,48E-05	1,00E+08	0,2235

Result of test:

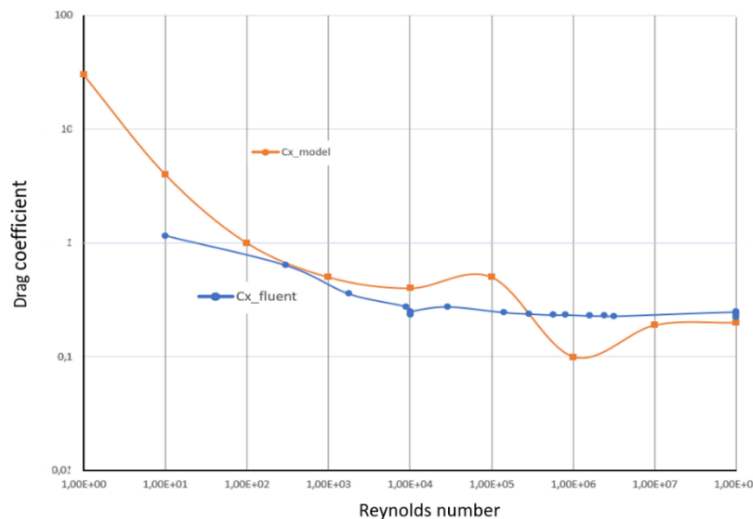


Figure 2.3 Graphic of Sphere drag coefficient function of Reynolds number

Remarks:

The orange curve is the exact answer.

The blue one is the curve found by the processing.

The two curves are really close to each other, considering that the scale is double logarithmic.

2.3.5. Validation of test

As just explained, the curve provided by calculation is close to the theoretical curve. Another satisfactory point about the process of calculus is that value of the drag force function of the Reynolds number is constant. The test has been done for two values: $Re = 10^4$ and $Re = 10^8$. Both tests gave points very close to each other, respectively for each Re value.

Thus, the calculus processing and the fluent simulation via Solidworks can be validate, and start working on trajectory controllers.

2.3 Falcon 9's grid fin

Firstly, it is necessary to define the limits of the system, especially regarding the size that needs to be small compared to the structure. The goal of this study is to provide ideas that could improve existing RLV. Secondly, the aerodynamic shape of the trajectory controller should disturb the less as possible the global aerodynamic shape of the RLV during the takeoff phase. During this phase the drag force has to be minimum. Another important requirement to bear in mind, the friction with the atmosphere provides a high temperature of the trajectory controllers and they have to resist against it. This raises the question of what material is the most suitable under such extreme conditions?

2.3.2. Grid fins idea

First question; how the grid fins work? The technology of grid fins is pretty old; it was used to control the trajectory of some Russian missiles (photos below). Today the technology is out of date for controlling missile trajectory, preferring rather fins or tails because the drag force of these control systems is very low compared to the drag force of the grid fins.

It is this last point on the drag force that the engineers of Space X have been interesting to use to decrease the velocity of the RLV during the reentry phase. If the trajectory has to be controllable as for the missile, the second aim of this control system is to be able to increase the drag force. They managed successfully to adapt this technology on Falcon 9 booster. The position, size, and material of this Space X grid fins will be studied. That will provide useful information for the next models.



Figure 2.4 Grid fins on soviet missiles, Military History Museum of Artillery, Saint-Petersburg

2.3.3. Falcon 9's structure

As you can see in *Figure 2.6*, the shape of the Space X grid fins is pretty close to the initial shape used by the old Russian missiles. However, the size has been scaled to the size of the Falcon 9 structure. These grid fins control the reentry trajectory via rotation as shown in *Figure 2.7*. Surprisingly they are four, where three would be theoretically enough to control it. However, four allow to increase more the drag force and simplify the reentry control from a programming point of view, with two control axis pitch and roll.

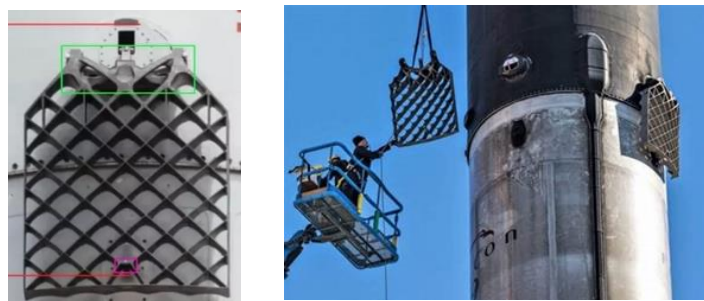


Figure 2.5 Space X grid fins during assembly on Falcon 9, Texas

In the description of each phase of the trajectory controller, *Figure 2.7*, the black arrow shows the velocity vector. During the take-off phase (case N°1), the grid fins are folded, and they are blocked close to the RLV pipe; the drag force is minimized. During the re-entry phase after the loop maneuver (case N°2), the grid fins can be deployed to increase the drag force and they stabilize the fall thanks to the high position of grid fins on the structure (detailed below). When the atmosphere is very dense, each grid fin can rotate to target the landing pad (case N°3).

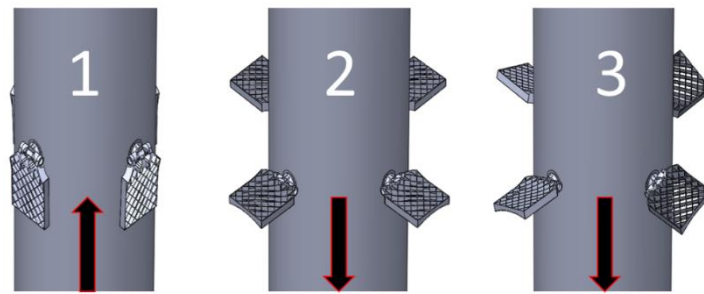


Figure 2.6 Three positions of Space X's Grid fins on Falcon 9

To test the different trajectory controllers, one 3D model of the Falcon 9 has been built, following the dimension presented in *Figure 2.8*. Every trajectory controller will be placed on the same position on the structure, which means at 5 meters from the top of the rocket. This position gives stability to the RLV as a simple pendulum [33], because the center of force is placed on the top of the center of inertia [34]. This structure will be also used for the next chapter, the Falcon 9 booster is our reference structure during whole this paper.

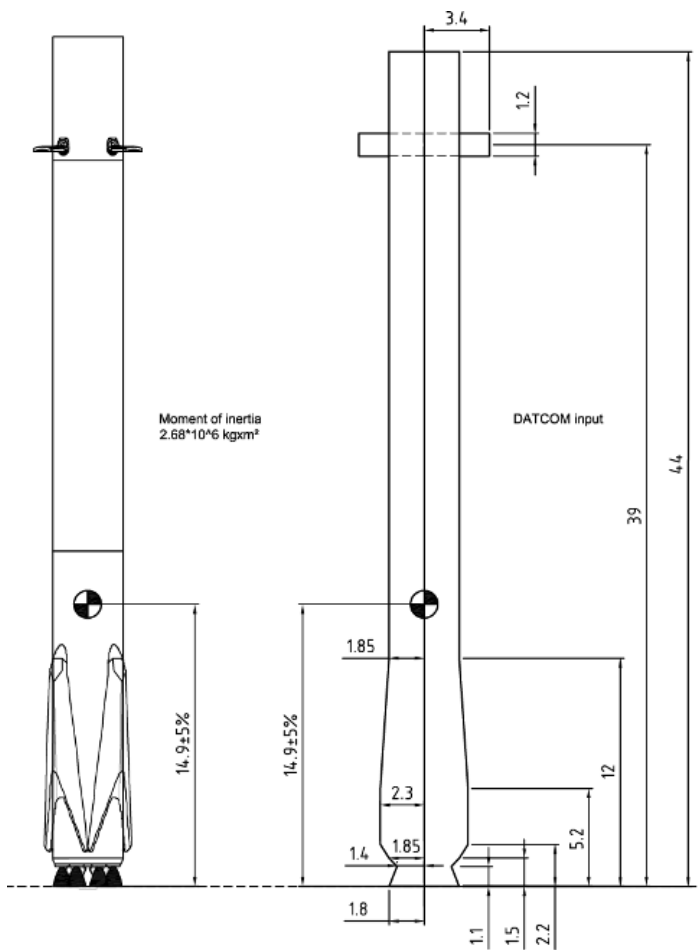


Figure 2.7 Real and model of Space X Falcon 9 booster

2.4 Trajectory controllers

2.4.1. Comparison

To compare the different trajectory controllers, a list of criteria is detailed as follows: note that all of them will be checked to select the best trajectory controllers. Some parameters are fixed to be able to compare comparable devices.

To know the characteristic of the trajectory controller it is necessary to know the evolution of the drag force and control force function of the angle of correction.

Validation criteria:

1. Level of drag force during reentry.
2. Level of control force, and linearity of control.
3. Low level of drag force during takeoff phase.
4. Temperature of air brake less than fusion point.
5. Weight
6. Size
7. Cost

Fixed parameters:

1. Material: Titan Ti-6242 [10] (as used by Space X for Grid fins)
2. Constant surface of contact: $S_0 = 1.427 \text{ m}^2$
3. Velocity is fixed, $V = 1650 \text{ m.s}^{-1}$

2.4.2. Possible improvement

Firstly, Space X's choice has to be understood, to have selected grids for the trajectory controller. The same global shape of grid fin but without the grid (no air would go through) has been tested. Secondly, the most used device to decrease the speed during atmospheric reentry is a parachute. So, one model has the parachute or bell shape. The inside area of this bell has the same size as other proposed models.

Thirdly, a simple fin is probably not the best device to decrease the velocity of the RLV. However, it could be very efficient for the trajectory control and the linearity of control.

Name of new idea:

Model 1: Flat brake Model 2: Bell brake Model 3: Simple fin

The result of force given by Flow simulation is on y axis and z axis of the parts. To determine the drag force and lift force, it is necessary to apply a basic change, detailed below.

Relation between Force Z, Force Y and Drag/Lift force:

By applying of the 2D basic change matrix:

$$P_{RLV,Velocity} = \begin{pmatrix} \cos(\alpha) & \sin(\alpha) \\ -\sin(\alpha) & \cos(\alpha) \end{pmatrix} \quad (2.3)$$

$$\begin{pmatrix} Drag_{force} \\ Lift_{force} \end{pmatrix} = P_{RLV,Velocity} \begin{pmatrix} Force Y \\ Force Z \end{pmatrix} \quad (2.4)$$

Thus:

$$Drag_{force} = F_y * \cos(\alpha) + F_z * \sin(\alpha) \quad (2.5)$$

$$Lift_{force} = -F_y * \sin(\alpha) + F_z * \cos(\alpha) \quad (2.6)$$

Thanks to the relation (1.5) and (1.6) the results are on the velocity axis for the drag and perpendicular to the velocity axis for the lift. The drag and lift forces generated by the flight controller are present in the following parts (2.4.3, 2.4.4, 2.4.5 and 2.4.6) and analysed and compared in the part (2.4.7 and 2.4.8)

2.4.3. Grid fin

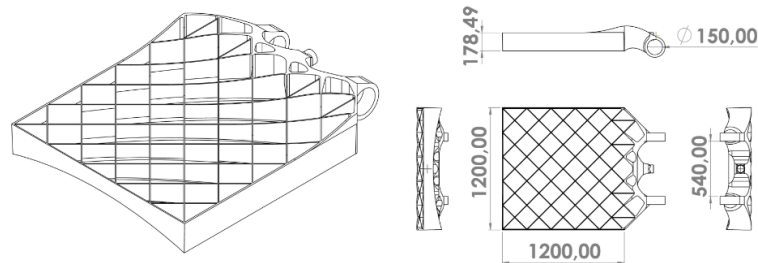


Figure 2.8 Space X grid fins, 3D model

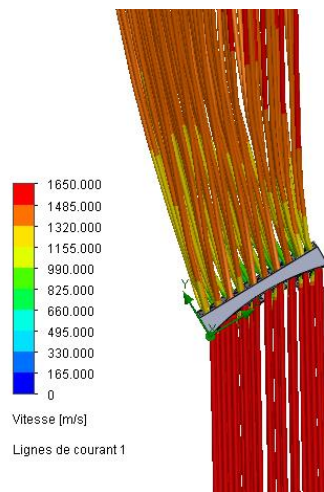


Figure 2.9 Flow simulation: Air flux around Grid fin with 30° of control

Table 2.2 Force generated by the grid fin.

Angle	Drag force	Lift force
0	1,84E+05	0,00E+00
5	1,92E+05	1,45E+05
10	2,27E+05	2,61E+05
15	2,95E+05	4,06E+05
20	3,98E+05	5,49E+05
30	7,45E+05	9,15E+05
40	1,49E+06	1,40E+06
50	8,74E+05	4,97E+05

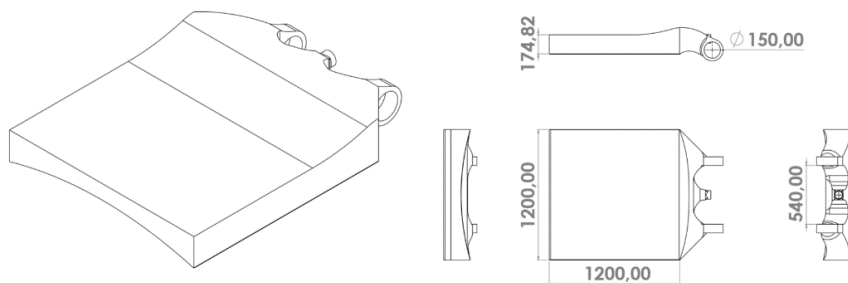


Figure 2.10 Flat fin, 3D model

2.4.4. Flat fin

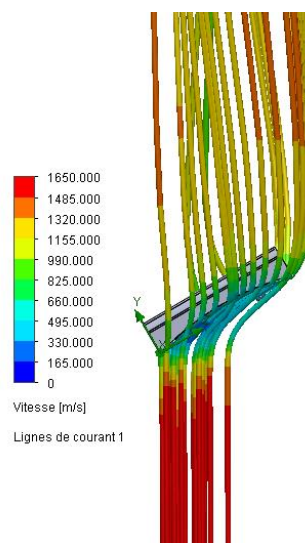


Figure 2.11 Flow simulation: Air flux around Flat fin with 30° of control

Table 2.3 Forces generated by the Flat brake

Angle	Drag force	Lift force
0	4,43E+06	0,00E+00
5	4,25E+06	2,42E+05
10	4,08E+06	6,47E+05
15	3,98E+06	9,37E+05
20	3,78E+06	1,20E+06
30	3,45E+06	1,77E+06
40	2,86E+06	2,10E+06
50	2,19E+06	1,92E+06

2.4.5. Bell brake

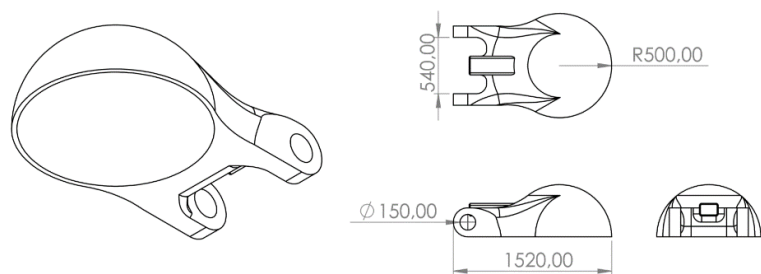


Figure 2.12 Bell brake, 3D model

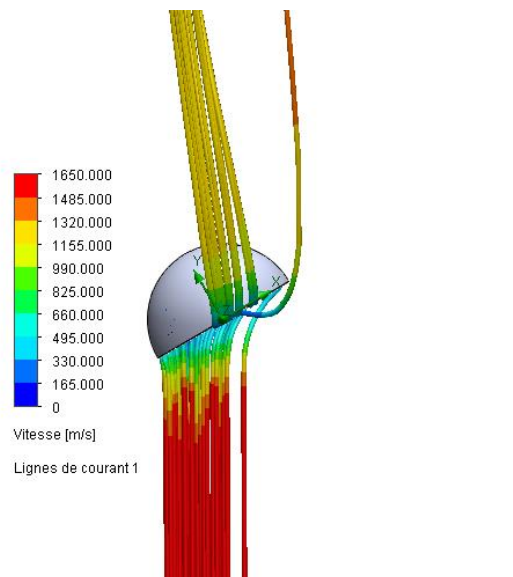


Figure 2.13 Flow simulation: Air flux around Bell brake with 30° of control

Table 2.4 Forces generated by the Bell brake

Angle	Drag force	Lift force
0	2,84E+06	0,00E+00
5	2,79E+06	1,51E+05
10	2,65E+06	3,26E+05
15	2,46E+06	4,67E+05
20	2,33E+06	5,91E+05
30	2,38E+06	8,85E+05
40	1,99E+06	1,03E+06
50	1,57E+06	8,49E+05

2.4.6. Simple fin

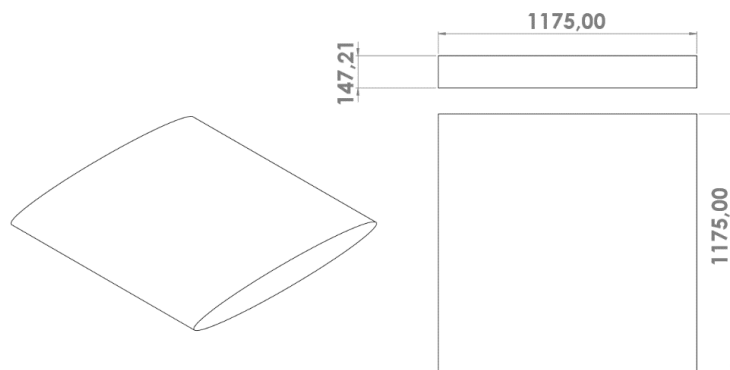


Figure 2.14 Simple fin, 3D model

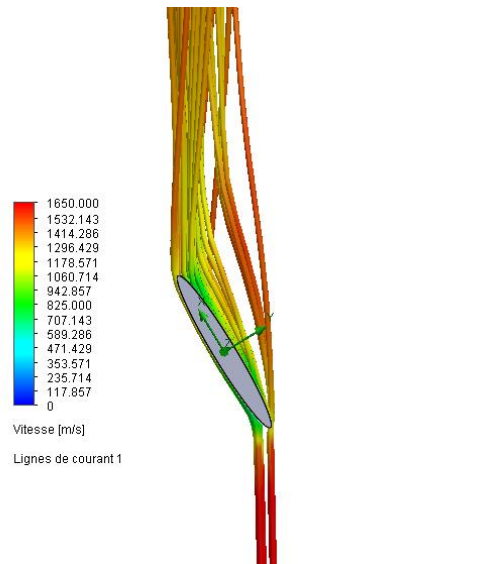


Figure 2.15 Flow simulation: Air flux around Simple with 30° of control

Table 2.5 Forces generated by the Simple fin

Angle	Drag force	Lift force
0	9,76E+04	0,00E+00
5	1,49E+05	1,97E+05
10	1,59E+05	3,65E+05
15	2,47E+05	5,55E+05
20	4,05E+05	7,58E+05
30	7,80E+05	1,14E+06
40	1,43E+06	1,51E+06
50	2,11E+06	1,62E+06

2.4.7. Strength of materials

Before comparing these trajectory controllers, it is important to remind that some values of drag force are very high and it is no sure that all materials can resist these efforts. The two trajectory controllers which generated the highest drag force are the Bell brake and the Flat fin. It is necessary to test them to know if they can resist these efforts. For the Grid fin and the Simple fin, the drag forces are much lower. We know that Grid fin works, as Space X proved it.

Thus, the tests are done via the Solidworks with Simulation complement, the material selected is the same as the one used by Space X for its Grid fins: The Titan Ti-6242. The force of pressure applied to the inferior surface of the trajectory controller is detailed below.

$$P_{Flatfin} = \frac{F}{S_0} = \frac{4.43 \times 10^6}{1.427} = 3.10 \times 10^6 \text{ N.m}^{-2} \quad (2.7)$$

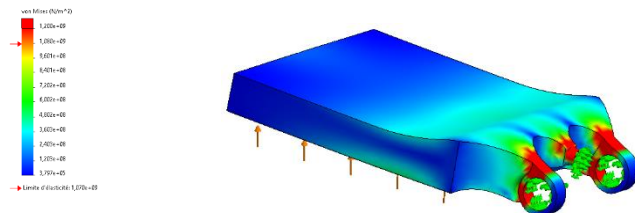


Figure 2.16 Simulation of effort applied by air on the Flat fin for control angle = 0°

$$P_{Bellbrake} = \frac{F}{S_0} = \frac{2.84 \times 10^6}{1.427} = 1.99 \times 10^6 \text{ N.m}^{-2} \quad (2.8)$$

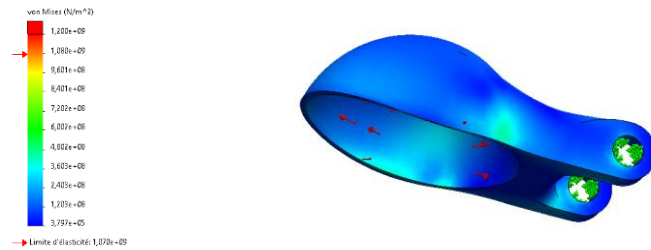


Figure 2.17 Simulation of effort apply by air on the Bell brake for control angle = 0°

For the Flat fin, the titan elastic limit has been reached: this structure cannot resist these efforts. About the Bell brake it is better. However, it is important to keep in mind the high temperature in which these devices are working. These tests have been made with titan temperature equal to 15°C while in reality it reaches 1000°C.

2.4.8. Results and comparison

Firstly, the comparison of drag force of every trajectory controller:

Table 2.6 Drag force for every trajectory controller

Angle	Flat fin	Bell brake	Grid fin	Simple fin
0	4,43E+06	2,84E+06	1,84E+05	9,76E+04
5	4,25E+06	2,79E+06	1,92E+05	1,49E+05
10	4,08E+06	2,65E+06	2,27E+05	1,59E+05
15	3,98E+06	2,46E+06	2,95E+05	2,47E+05
20	3,78E+06	2,33E+06	3,98E+05	4,05E+05
30	3,45E+06	2,38E+06	7,45E+05	7,80E+05
40	2,86E+06	1,99E+06	1,49E+06	1,43E+06
50	2,19E+06	1,57E+06	8,74E+05	2,11E+06

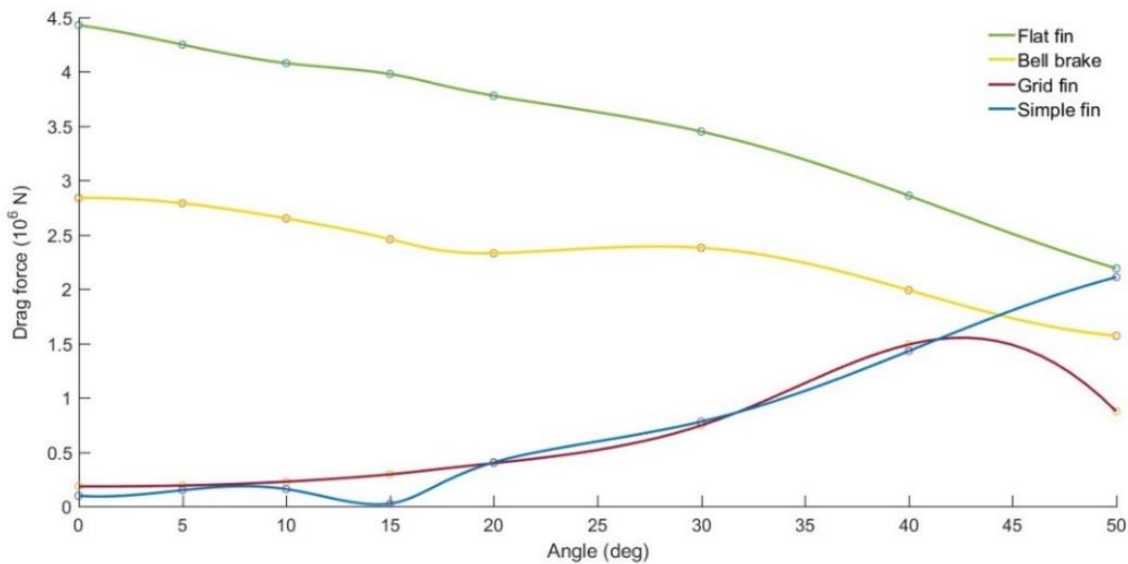


Figure 2.18 Graph of drag forces generated by every trajectory controller

Comment

As expected, the Bell brake and the Flat fin generated more drag force. However, as just explained both solutions are not possible because the strength of the material is not high enough to resist to these efforts. The two other proposals, the grid fin and the simple fin, generated the same drag effect.

Table 2.7 Lift force generated by every trajectory controller

Angle	Flat fin	Bell brake	Grid fin	Simple fin
0	0,00E+00	0,00E+00	0,00E+00	0,00E+00
5	2,42E+05	1,51E+05	1,45E+05	1,97E+05
10	6,47E+05	3,26E+05	2,61E+05	3,65E+05
15	9,37E+05	4,67E+05	4,06E+05	5,55E+05
20	1,20E+06	5,91E+05	5,49E+05	7,58E+05
30	1,77E+06	8,85E+05	9,15E+05	1,14E+06
40	2,10E+06	1,03E+06	1,40E+06	1,51E+06
50	1,92E+06	8,49E+05	4,97E+05	1,62E+06

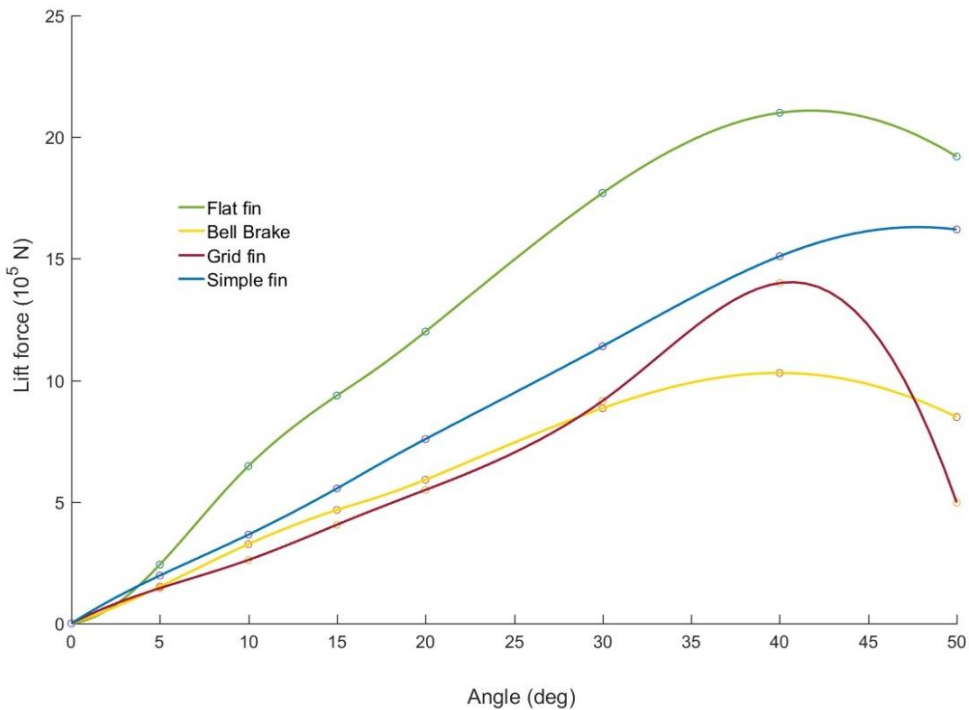


Figure 2.19 Graph of lift force generated by every trajectory controller

Comment

If the results of the drag force were predictable, this time for the lift/control it was less intuitive to forecast. *Figure 2.19* shows that the Flat fin generates the higher control force, as explained previously this flight controller is not available due to the too high-level force of the drag. The second one who generated the more control force is the simple fin. Better than the Space X's Grid fin. Another interesting point about the Simple fin is that the function linking the lift/control force and angle of correction is linear. Thus, it will be easier to programming the control program using a function like the (2.9).

$$\text{Lift. force}(angle) = 3.5468 \cdot 10^4 * angle \quad (2.9)$$

In view of these two observations, the model called "Simple fin" seems to be the most suitable. It will be our flight controller for the rest of this paper.

2.4.9. Final model

The result of this test showed that the best trajectory controller is the Simple fin. All requirements have been fulfilled: high level of control force, low level of drag during the take-off phase, light structure, and simplicity to machining. There is only one point for which this device has not a good score: the drag force directly generated. It will be explained in the next chapter how the control force given the attack angle to the whole structure generates a lot of drag.

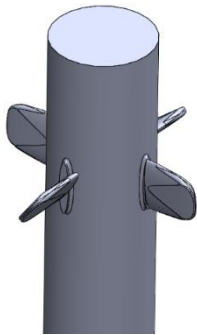


Figure 2.20 Simple fin on the RLV



Figure 2.21 Fins assembled on the Space X Starship

Even if Space X is confident to use the grid fin, for the Starship project they have decided to shift to a kind of Simple fin trajectory controller.

2.5 Global review of RLV shape

The previous survey showed that “Simple fins” were the best idea to control the trajectory. However, an ideal trajectory controller may have another kind of shape, and perhaps not an additional part like a fin. To get the ideal shape of RLV, one idea is to review the global shape of the RLV. However, according to aerospace engineering, the global shape of LV is a cylinder. In the first part, the top of a perfect cylinder will be reviewed to improve the drag force. Secondly, a general review will be presented named “Air to Air brake”, this one take into account the cylinder consideration but with a new engineering solution.

2.5.1 Top shape of RLV

Modify the top of the rocket is one way to improve the drag force of the RLV while keeping a stable RLV. The main requirement for these tests is the realistic aspect. Here the control consideration is not taken into account. Thus, four models have been designed and tested: the first one is a simple cylinder (according to Falcon 9’s dimensions). The next models have the same base cylinder modified with some drag shape improvements. By order (right to left on Figure 2.22) the second aims to use the cavity effect, the third one using the parachute effect, the last one aims to generate the more diameter variation to create turbulence.

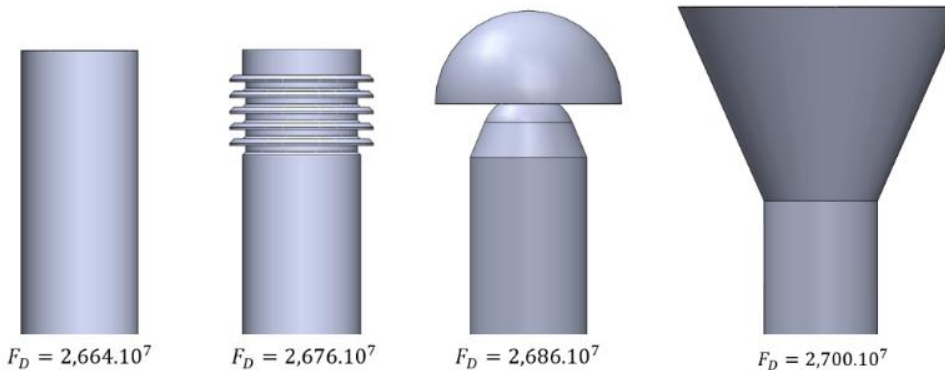


Figure 2.22 Different kind of shape for the top of RLV with Value of drag force

At first glance the result looks strange and somewhat disturbing. It does not fit well. Logically, the major air resistance from the bottom of the RLV comes from the perpendicular surfaces of air flux. It suggests once more that the rocket has to take attack angle to increase significantly the drag.

2.5.2 Air to Air brake

One ambitious target has been developed: the air/air brake. This trajectory controller aimed to use the air flux around the rocket to control the trajectory. This air flux is captured in the middle of the structure, going through the RLV inside pipes and ejected via the elbow controllers. The following view present the RLV structure with the air-air brake system.

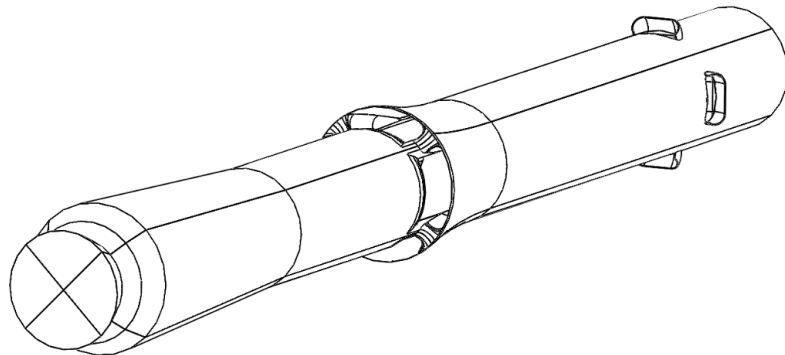


Figure 2.23 Air Air Structure

To control the RLV, the control method is close to the method presented previously. Here the rotation of fins to generated more lift force is replaced by the rotation of elbow to directing the airflow.

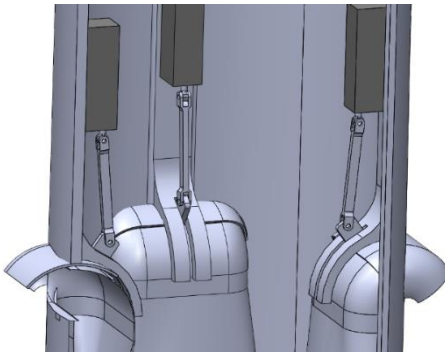


Figure 2.24 Mechanism of elbow

One representation of the airflow who pass-through of the structure is presented in the following figure, the air pass firstly on the air horn, then pass of one pipe inside the RLV before by eject with variable angle with the elbow.

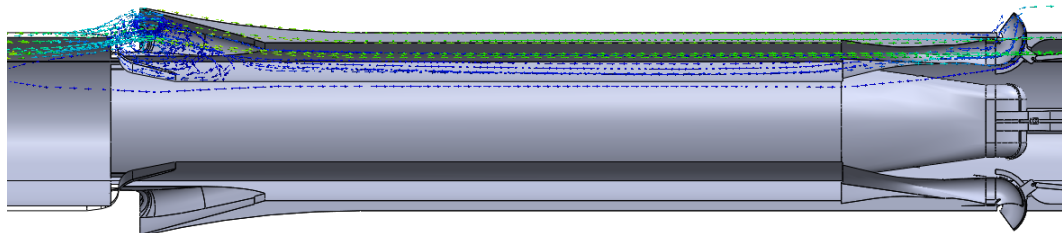


Figure 2.25 Air flow through of the structure

To understand more the working of the “Air to Air brake” a simulation of the airflow is presented in *Figure 2.26*. However, the result is not enough efficient to be able to works, this theoretical structure can work s only is the pipe inside the RLV are very large. Thus, it is not according to RLV requirements, this place is saved for the propellant.

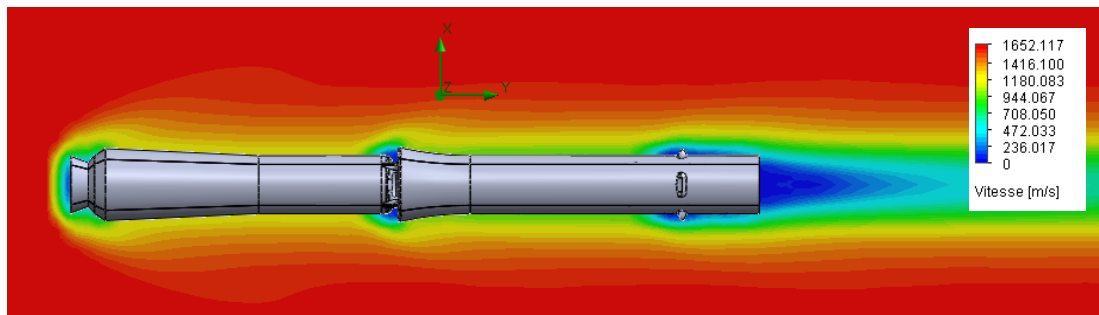


Figure 2.26 Flow simulation: Air flux around RLV with air to air brake

2.6 Rotary idea to keep RLV balance

2.6.1 Personal idea

This last part of this chapter has for aim to introduce one more interesting notion never mentioned before and pretty rare in aeronautical or astronautical engineering; the inertial force of rotation. The reason of this rare usage, is that most of the time engineers want to avoid it, because the rotation of the RLV provide many issues of control, even if this rotation is on the yaw axis. I agree with them but the question is how to use the inertial force of rotation without making RLV rotating? In other words: it is the airflow around the RLV that will turn. The airflow will be not around but will go through the RLV. The goal of the airflow is to provide stability of the rocket around the velocity axis.

To validate this idea and check the efficiency of this suggestion, a model has been developed, far from the size of the aerospace structure, and far from the speed of air during reentry as using water instead.

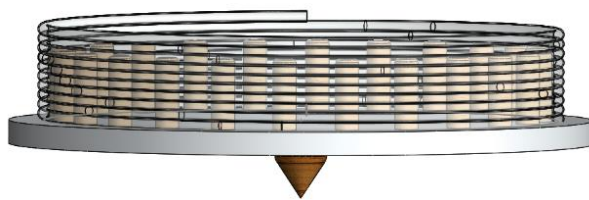


Figure 2.27 Water Spinning top 3D model



Figure 2.28 Water Spinning top and water pressure device

After many tests, the spinning did not keep well the balance, however, an important inertial effect is noticed when the water flow is passing through of the pipe but not high enough. That should work with a faster velocity of water flow.

To check if this process makes sense during the reentry phase, a comparison between the constructed model and a potential RLV must be carried out. The Falcon 9's dimensions is selected, and the Reynold number is used as comparing tool.

$$Re = \frac{\rho \cdot V \cdot L}{\mu} \quad (2.10)$$

The two Reynold numbers are calculated to compare the order of magnitude.

The velocity of each system has to be found, for the RLV the usual reentry speed will be selected, for the spinning top during the test it was 1 m.s^{-1} , by estimation ten time more will give efficiency to the water.

$$V_{water} = 10 \text{ m.s}^{-1} \quad (2.11)$$

$$V_{air} = 1650 \text{ m.s}^{-1} \quad (2.12)$$

For the dimension number noted L it will be the length of the pipe

$$L = N_{pipe} * Length * Diameter \quad (2.13)$$

$$L_{ST} = 1 * 20 * 2 * \pi * 0.01 = 1.256 \quad (2.14)$$

$$L_{RLV} = 4 * 50 * 2 * \pi * 0.8 = 1005 \quad (2.15)$$

$$Re_{spinning_top} = \frac{\rho_{water} \cdot V_{water} \cdot L_{ST}}{\mu_{water}} = \frac{997 * 3 * 1.256}{1.10^{-3}} = 3.7 * 10^6 \quad (2.16)$$

$$Re_{RLV} = \frac{\rho_{air} \cdot V_{air} \cdot L_{RLV}}{\mu_{air}} = \frac{1.225 * 1650 * 1005}{1.81 \cdot 10^{-5}} = 1.12 * 10^{11} \quad (2.17)$$

To summary this idea should work for a huge pipe when the air velocity is very high. However, that makes no sense to transport this kind of structure in the space, as it would be too heavy and would take too much place, for a final result not that helpful. Likely, this idea can be developed for another application.

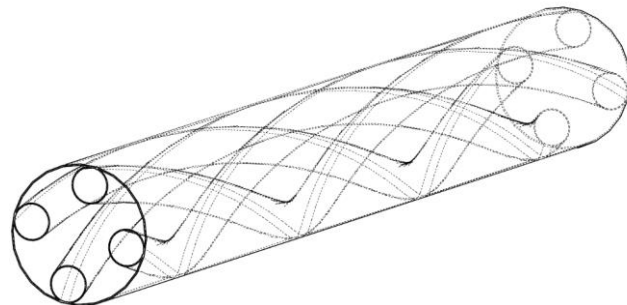


Figure 2.29 Model of air flux rotation

2.6.2 Other ways to use rotary recovery system

The usage of a propeller-like a helicopter is acceptable to keep the balance and the vertical path during the reentry phase, and enjoys a high drag effect due to the rotation. NASA was interested in this kind of device [35] two decades ago as well as a private company [36]. Without real success, this process has been forgotten.

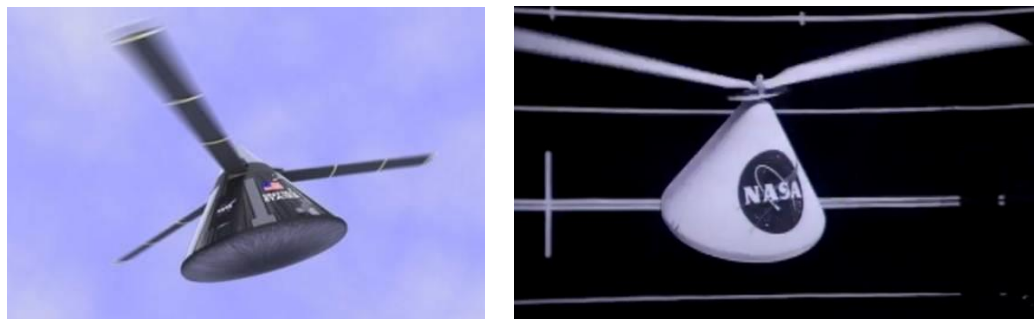


Figure 2.30 Parachute rotor blade system



Figure 2.31 Rotary rocket

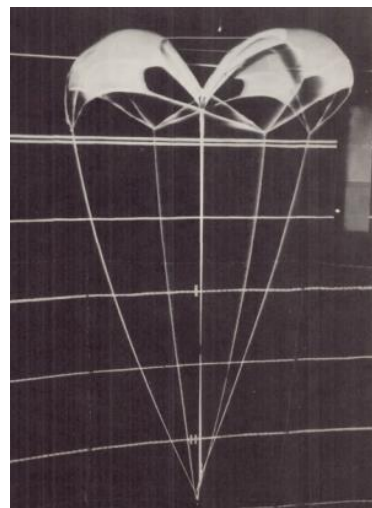


Figure 2.32 Rotary parachute

Another project from Nasa used the rotation to decrease the velocity during the end phase control of reentry; with parachute this time. All of these projects showed the interest of the rotation to dissipate the gravity energy. This idea is presented in chapter 3 though with another form, but looking after the same goal.

2.7 Conclusion

This first chapter shows us the complexity of bringing a rocket back to earth. Many projects have been abandoned, due to too many difficulties to be solved. If the Space X company is successful today, it is also because of its reliability. Thus, it is necessary to find a reliable and therefore simple system for a complex challenge. Controllers as grid fins have to be trajectory controller more than adding drag force to the system. Thus, the simple fin controller design is selected, more power to control, and thus allows the desired angle of attack to the rocket.

Chapter 3 Trajectory design and simulation

3.1 Introduction

The reentry optimization has two ways of improving: engine use and the attack angle [37]. In this case, it will be the improvement of using the attack angle. Many interesting studies exist about it. Wishing to bring something new, this study will be in 3 dimensions and around a trajectory line. The aim is to improve the drag force without change the position of the gravity/inertia center.

To make an accurate simulation, many points have to be checked. First of all, by applying Newton 2nd law the physical relations will be found. Then, it is necessary to know the variation of air density function of the altitude, thus the atmosphere has to be modeled. Thirdly, the variation parameter is the attack angle, this one varying the aerodynamic forces. It is essential to know this rate of variation. That means be able to reply; how the drag force is and the lift force is for 10° of attack angle. Knowing all of that, some simulations can be run to understand how the RLV reacts function of the angle attack. In the end different ideas of reentry will be presented.

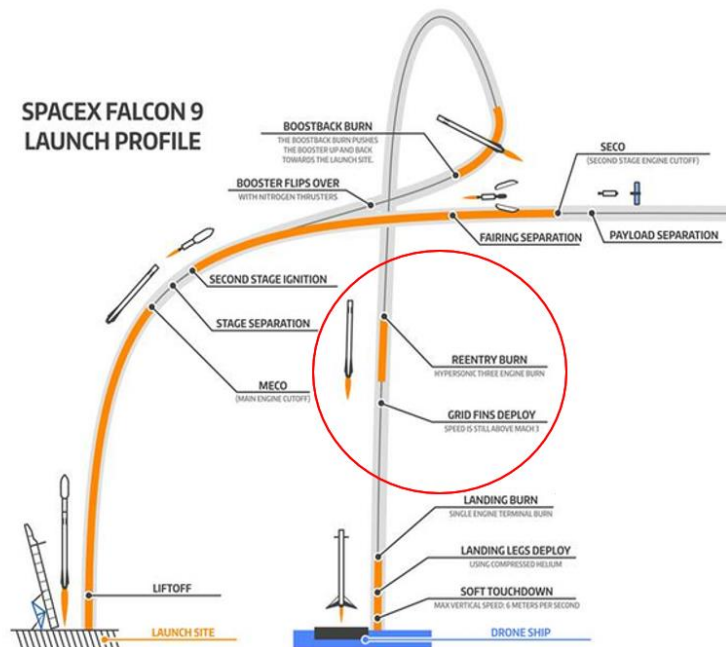


Figure 3.1 Graphic representation of the trajectory steps of the booster of the falcon 9

3.2 Background and Objectives

Since the beginning of space travel, the cost has been the key factor. That's why the research to reuse the booster of LV has been so extensively studied by the space launch companies. It is a real optimization in cost savings. Today this process becomes a routine for the Space X team. Nonetheless, looking for further improvement is in all minds. The crux remains the cost and in space language it means the lowest weight, in other words, the lowest fuel usage to cover the needs. That's still true with RLV though one additional consideration has to be computed: the drag force, the "enemy" during the takeoff phase as extremely costly in fuel consumption. Many surveys have developed the optimization in engine utilization during the reentry phase [27,28]. Another axis of study is the optimization of the attack angle to get the best drag force to consume energy [24]. It is this axis of improvement that will be studied. Most of the time these simulations are done in 2 dimensions, the objective is to make it in a 3D simulation.

The results obtained in the previous chapter will be useful as the trajectory controller will be used to control the RLV during this reentry phase. According to the result in chapter 1, Simple fins are selected. The structure of the Falcon 9 will be used as the calculation base for the aerodynamic tests. The purpose of the aerodynamic tests will be to determine the drag and lift force values as a function of the angle of attack. Thereafter several methods of re-entry will be developed, which aim to consume the maximum amount of energy via these aerodynamic forces.



Figure 3.2 The re-entry burn of SpaceX Falcon 9's first stage

3.3 Equation of trajectory control

In this study case, the RLV will not use the engine during this re-entry phase. The only way to control it will be via the trajectory controllers, this device has been explained and developed in the previous chapter. The distance that separates these devices from the center of the inertia of the RLV is the lever arm. This distance provides the force necessary for the trajectory controller to manage the angle of attack during the reentry phase. As for the

aerodynamic forces, they are directly dependent on the speed vector, in value but also in direction, so the drag force is on the same axis as the speed, the lift is perpendicular to the drag.

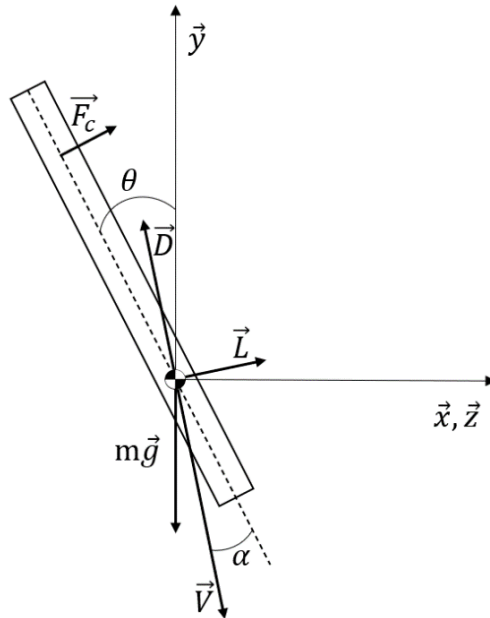


Figure 3.3 Mechanical model of RLV during reentry phase

Equations of the structure:

$$m \cdot \ddot{x} = -D \cdot \sin(\theta - \alpha) + L \cdot \cos(\theta - \alpha) + F_c \cdot \cos(\theta) \quad (3.1)$$

$$m \cdot \ddot{y} = -g + D \cdot \cos(\theta - \alpha) + L \cdot \sin(\theta - \alpha) + F_c \cdot \sin(\theta) \quad (3.2)$$

$$I \cdot \ddot{\theta} = \frac{L_{RLV}}{1.83} \cdot F_c \quad (3.3)$$

Remark:

The control force noted F_c is provided by the trajectory controller, this force corresponds to the lateral control force developed in the previous chapter.

The value of lever arm is the length of the RLV divided by 1.83. This coefficient comes from the Falcon 9's lever arm. The length of the Falcon 9 is 44 meters and the distance between the grid fin and the center of gravity is 24.1 meters. Thus $44 / 24.1 = 1.83$.

Aerodynamic forces equations:

$$D = q(y) \cdot S \cdot C_D(\alpha, V) \quad (3.4)$$

$$L = q(y) \cdot S \cdot C_L(\alpha, V) \quad (3.5)$$

$$q(y) = \frac{1}{2} \cdot \rho(y) \cdot V^2 \quad (3.6)$$

3.4 Air density function of altitude

The Earth's atmosphere is not constant. Therefore, it is necessary to take into account the density variation which depends on the variation in pressure and temperature, as Marcel Délèze developed in “Atmospheric mass by altitude according to barometric levelling model” [22].

From the ideal gas expression:

$$p \cdot V = n \cdot R \cdot T \quad (3.7)$$

$$\rho = \frac{m}{V} = \frac{m}{n} \frac{p}{R \cdot T} = \frac{M}{R} \frac{p}{T} \quad \text{with} \quad M = \frac{m}{n} \quad (3.8)$$

$$\rho = \frac{m}{V} = \frac{m}{n} \frac{p}{R \cdot T} = \frac{M}{R} \frac{p}{T} \quad (3.9)$$

$$\rho(y) = \frac{M}{R} \frac{p(y)}{T(y)} = \frac{M}{R} \frac{p_0}{T_{0-a.y}} \left(1 - \frac{a}{T_0} y\right)^{\frac{Mg}{Ra}} \quad (3.10)$$

Numerical application:

$$\rho(y) = \frac{28.966 \cdot 10^{-3}}{8.31451} \frac{101325}{(15+273.15)-6.5 \cdot 10^{-3} \cdot y} \left(1 - \frac{6.5 \cdot 10^{-3}}{15+273.15} y\right)^K \quad (3.11)$$

$$\text{with } K = \frac{28.966 \cdot 10^3 * 9.805}{8.31451 * 6.5 \cdot 10^{-3}}$$

After simplification:

$$\rho(y) = 352.995 \frac{(1-0.0000225577 y)^{5.25516}}{288.15-0.0065 y} \quad (3.12)$$

The variation of density known, as described above, the understanding of aerodynamic forces has evolved. Thus, it is possible to divide the reentry phase into two parts, before 40 km and under, in other words, before strong aerodynamic effects and after. The scope of the study will be between 40 km and the ground.

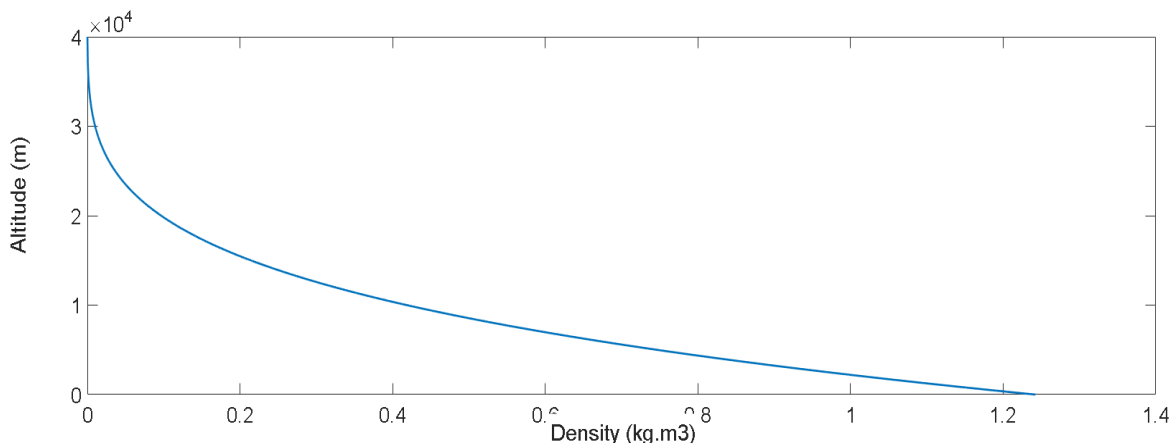


Figure 3.4 Air density function of altitude (from 4000 m to sea level)

3.5 Aerodynamic forces

To describe these two forces, two parameters must be taken into account, the attack angle and the speed. The attack angle is the angle between the RLV axis and the velocity vector. It is noted in Figure 3.3 and 3.5. The particularity of the case presented in Figure 3.5 is that the velocity vector is coaxial with the vertical axis, this specificity is used to simplify the future fluid dynamic study. This figure shows the test model used in Flow Simulation (Solidworks complement). The process is the same as used for the air brakes on the previous chapter. The purpose of this study is to understand the Falcon 9's reaction to the aerodynamic forces as a function of attack angle. The result has to be two functions that will provide the drag force and lift force function of the attack angle and the speed. However, the attack angle will be the only variable (from 0° to 80°), while the velocity will be kept constant with 1650 m/s. The aim is to develop a ratio method. The forces are detailed in Table 3.1.

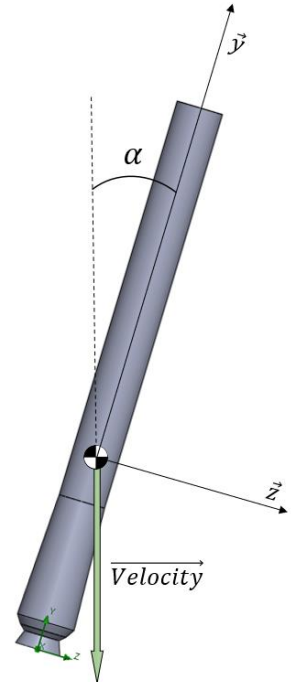


Figure 3.5
Flow simulation

Table 3.1 Forces applied on the RLV function of the attack angle

Angle	speed (m/s)	Speed on y	Speed on z	force total	force y	force z
0	1650	1650	0	2,65E+07	2,65E+07	1,57E+03
1	1650	1649,7487	28,7964706	2,63E+07	2,63E+07	6,68E+05
3	1650	1647,73873	86,3543277	2,55E+07	2,55E+07	1,59E+06
5	1650	1643,72125	143,806975	2,62E+07	2,60E+07	3,49E+06
10	1650	1624,93279	286,519493	2,80E+07	2,55E+07	1,15E+07
15	1650	1593,77761	427,051424	3,69E+07	2,56E+07	2,66E+07
20	1650	1550,49282	564,333236	5,31E+07	2,56E+07	4,65E+07
25	1650	1495,40785	697,320131	7,41E+07	2,59E+07	6,95E+07
30	1650	1428,94192	824,999999	9,87E+07	2,55E+07	9,54E+07
40	1650	1263,97333	1060,59955	1,56E+08	2,27E+07	1,54E+08
50	1650	1060,59956	1263,97333	2,14E+08	1,66E+07	2,13E+08
60	1650	825,000002	1428,94192	2,68E+08	1,08E+07	2,68E+08
70	1650	564,333239	1550,49282	3,11E+08	6,43E+06	3,11E+08
80	1650	286,519496	1624,93279	3,10E+08	3,14E+06	3,09E+08

The results of the study show two forces, the force on the axis y and z. However, both of these axes are specific to the RLV, it is not the drag force axis and the lift force axis. The graphic below details these two forces function of angle in degrees.

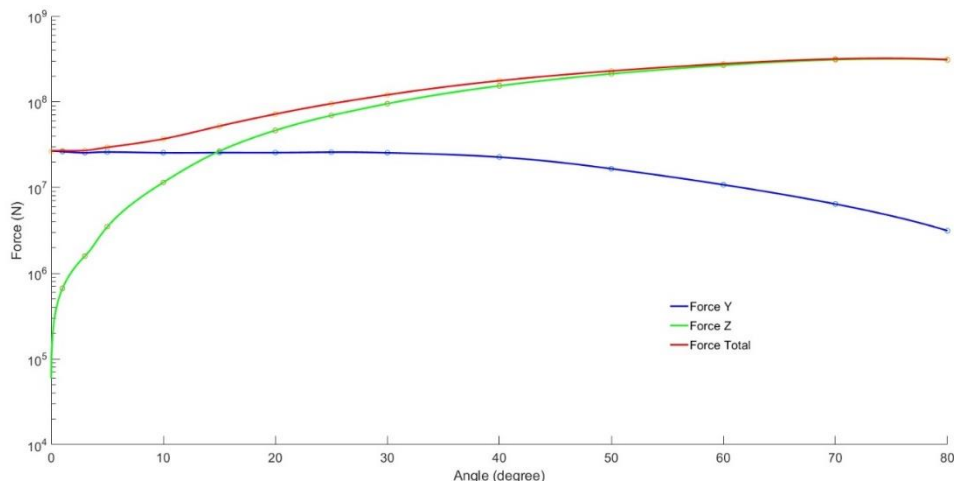


Figure 3.6 Force applied to the RLV function of the attack angle

Naturally the force on the z axis does not exist if the attack angle is equal to zero. Note that when the attack angle reaches 35° the forces are equal. Thus, the energy consumed during the reentry phase is directly linked to the attack angle and increased logically. Before finding these ratios, it is necessary to know the drag force and the lift force, they are components of force z and force y (Annex 3.1).

By applying of the 2D basic change matrix detailed on the chapter 2, equation (2.3) To resume the previous result the drag and lift force relation are developed below:

$$Drag_{force} = F_y * \cos(\alpha) + F_z * \sin(\alpha) \quad (3.13)$$

$$Lift_{force} = -F_y * \sin(\alpha) + F_z * \cos(\alpha) \quad (3.14)$$

The aerodynamics forces are not useful for the values, firstly because they depend on exact values of angles. Secondly, these values are only available for the Falcon 9's dimensions. To use these values, it is necessary to do polynomial regression of ratio. How to find the ratio? For the drag force is it quite simple it will be a comparison between the drag force with α attack angle and drag force with 0 attack angle. However, for the lift force this solution does not work because the lift force is null for 0 attack angle. Thus, the ratio will be a comparison between the lift force with α attack angle and drag force with the attack angle.

Table 3.2 Forces applied to the RLV and ratios function of the attack angle.

Angle	Force y	Force z	Drag force	Ratio/drag_force_0	Lift force	Ratio/Drag_force
0	2,65E+07	0,00E+00	2,65E+07	1	0,00E+00	0
1	2,63E+07	6,68E+05	2,63E+07	0,993	2,09E+05	0,008
3	2,55E+07	1,59E+06	2,55E+07	0,964	2,54E+05	0,010
5	2,60E+07	3,49E+06	2,62E+07	0,989	1,22E+06	0,047
10	2,55E+07	1,15E+07	2,71E+07	1,024	6,91E+06	0,255
15	2,56E+07	2,66E+07	3,16E+07	1,192	1,91E+07	0,605
20	2,56E+07	4,65E+07	4,00E+07	1,510	3,49E+07	0,873
25	2,59E+07	6,95E+07	5,28E+07	1,996	5,20E+07	0,985
30	2,55E+07	9,54E+07	6,97E+07	2,634	6,99E+07	1,002
40	2,27E+07	1,54E+08	1,17E+08	4,403	1,04E+08	0,888
50	1,66E+07	2,13E+08	1,74E+08	6,579	1,24E+08	0,715
60	1,08E+07	2,68E+08	2,38E+08	8,973	1,25E+08	0,525
70	6,43E+06	3,11E+08	2,94E+08	11,113	1,00E+08	0,341
80	3,14E+06	3,09E+08	3,05E+08	11,532	5,07E+07	0,166

To be able to use the ratio curves presented in *Figure 3.7* it is necessary to know the equations of these ones. To do that Polyfit/Polyval MATLAB functions [39], they will be useful for the modeling via MATLAB Simulink for the next part.

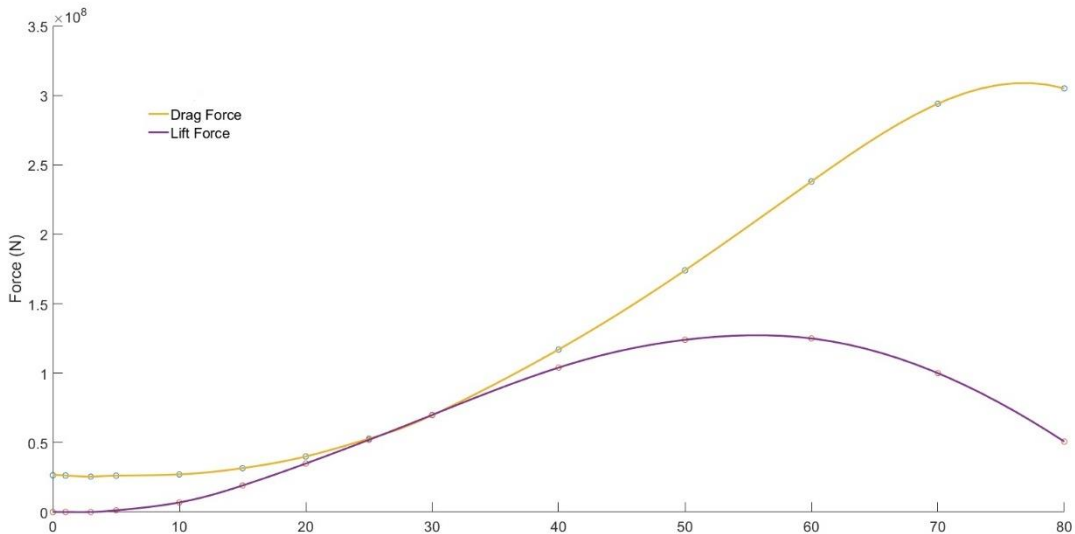


Figure 3.7 Drag and Lift force applied on the RLV function of the attack angle

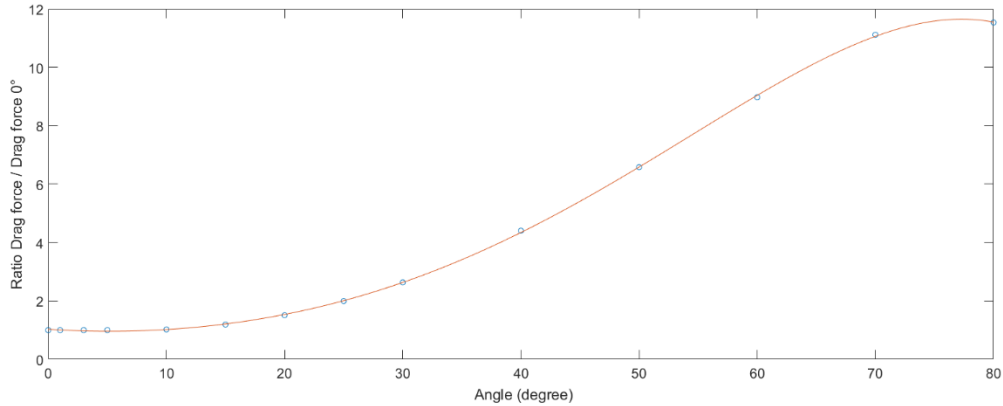


Figure 3.8 Ratio between drag force and drag force at 0°

$$\begin{aligned}
 \text{Ratio_1}(\alpha) = & -8.960867670155147 \cdot 10^{-9} * \alpha^5 + 8.358800253845612 \cdot 10^{-7} * \alpha^4 \\
 & - 1.924871868649280 \cdot 10^{-5} * \alpha^3 + 0.002765967864201 * \alpha^2 \\
 & - 0.027607288729840 * \alpha + 1.031924700936376
 \end{aligned} \tag{3.17}$$

Remark:

The previous equation is very close to reality but it is not a stable equation due to the high level of degree of the polynomial regression. Because of the shape of the curve it is possible to divide in two the polynomial regressions. It will give more stability for this model while keeping enough accuracy. The same process will be adopted for the ratio linked to the lift force.

Ratio curves and equations:

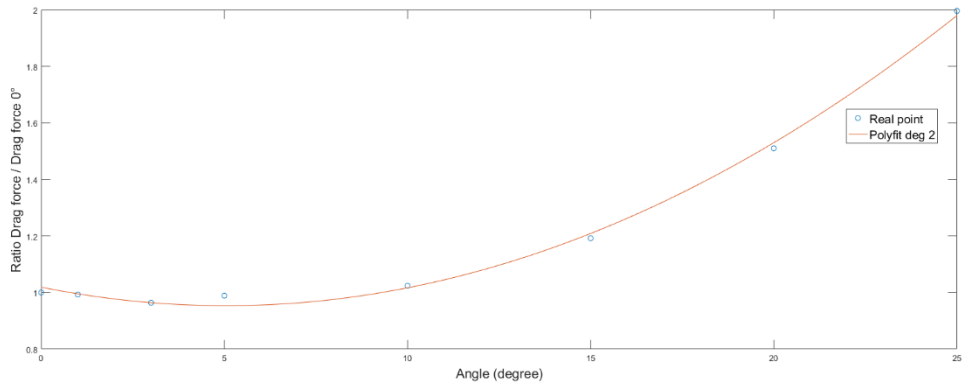


Figure 3.9 Ratio between drag force and drag force at 0° between 0° and 25° (-)

$$Ratio_2(\alpha) = 0.0026 * \alpha^2 - 0.0260 * \alpha + 1.0191 \quad (3.18)$$

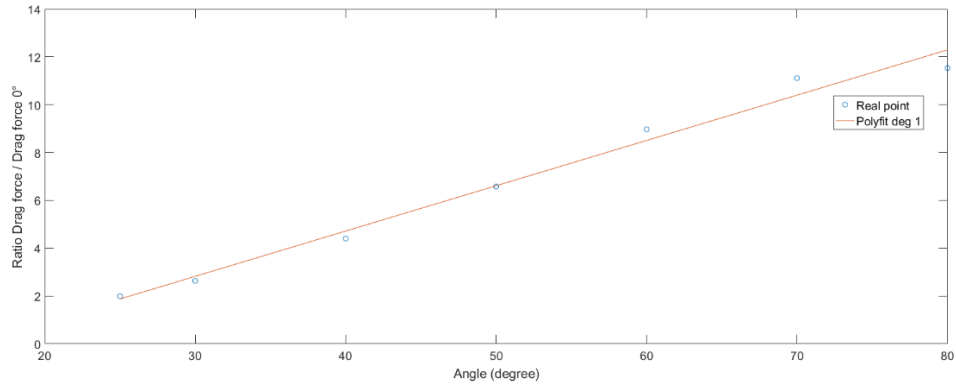


Figure 3.10 Ratio between drag force and drag force at 0° between 25° (+) and 80°

$$Ratio_3(\alpha) = 0.1894 * \alpha - 2.8591 \quad (3.19)$$

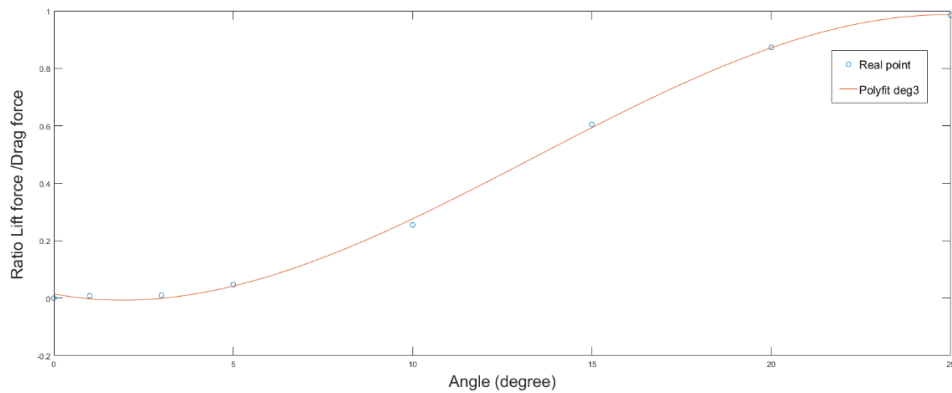


Figure 3.11 Ratio between lift force and drag force between 0° and 30° (-)

$$Ratio_4(\alpha) = -0.0002 * \alpha^3 + 0.0066 * \alpha^2 - 0.0234 * \alpha + 0.0148 \quad (3.20)$$

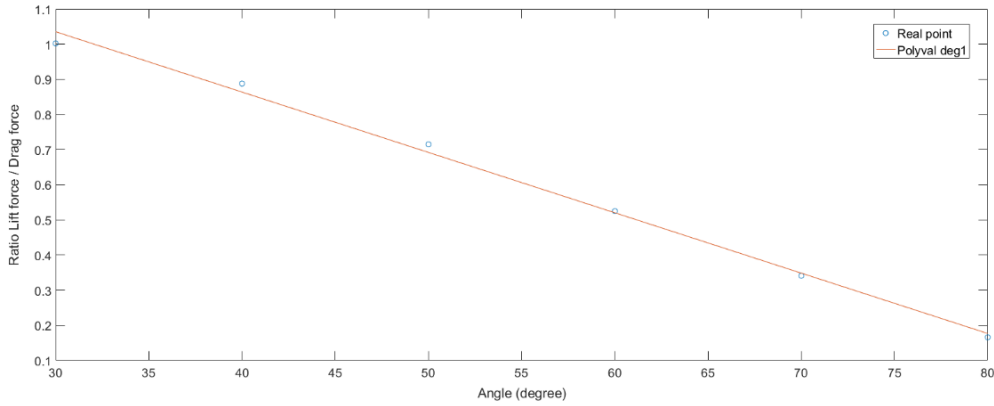


Figure 3.12 Ratio between lift force and drag force between 30° (+) and 80°

$$Ratio_5(\alpha) = -0.0172 * \alpha + 1.5508 \quad (3.21)$$

Now drag and lift forces are known for the angle range $[0^\circ, 80^\circ]$, keeping in mind that these ratios are found for Falcon's shape. They are relevant as well for other rockets with smaller or bigger dimensions as long as the shape remains the same. As the Falcon 9's shape is very close to a long cylinder, it corresponds to lot of rockets.

The speed dependence for the aerodynamic coefficients has not been studied, only the angle of attack dependence has been done. However, this method is based on a ratio, and all ratios depend on the drag force at 0° , and this one takes into account the speed.

To understand better the air reaction around the structure, it is necessary to see the velocity lines around the RLV. Attack angle influence on the temperature of the structure has to be checked too. To define these two requirements, two tests are presented in the following section for 0° and 20° of attack angle.

3.6 Velocity line and temperature visualization

The Falcon 9 model previously presented will be used. It will be subject to an air flux at 1650 m.s^{-1} for two attack angles, the verticality so $\alpha = 0^\circ$ and for $\alpha = 20^\circ$.

Velocity lines visualization:

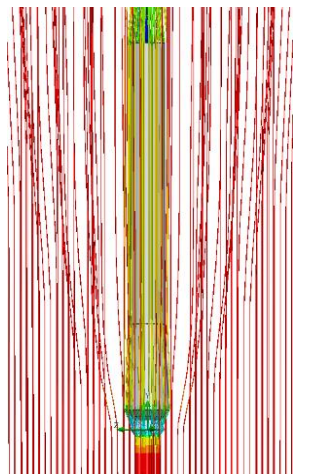


Figure 3.13 Velocity line for $\alpha = 0^\circ$

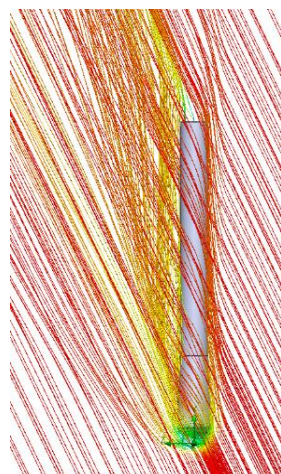
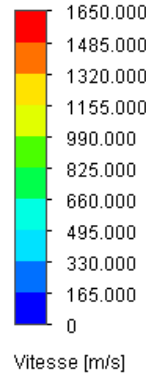


Figure 3.14 Velocity line for $\alpha = 20^\circ$

Visualization of temperature:

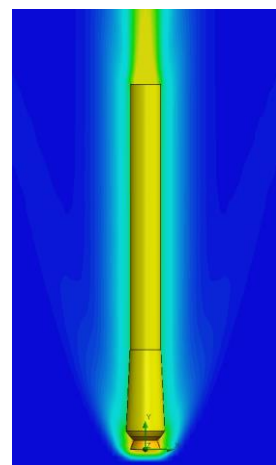


Figure 3.15 Temperature wake for $\alpha = 0^\circ$

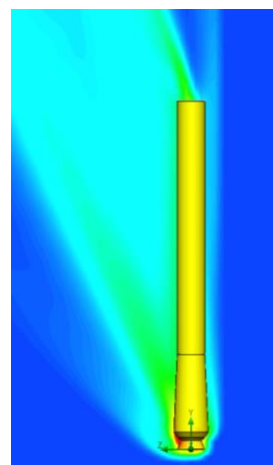
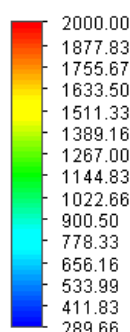


Figure 3.16 Temperature wake for $\alpha = 20^\circ$

$$T_{max} = 1707^\circ K$$

$$T_{max} = 1965^\circ K$$

One important point to note is the hottest point on the structure, if this one does not exist on the structure when $\alpha = 0^\circ$ due to the symmetrical flux around the structure and thanks to the temperature diffusion through of RLV. When $\alpha = 20^\circ$ the diffusion does not work enough.

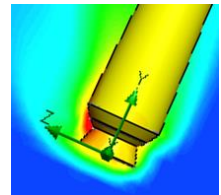


Figure 3.17 Warmer point for $\alpha = 20^\circ$

One thing has to be noted, it is the fact that the temperatures shown on the *Figures 3.15, 3.16, 3.17*, are surface temperature of structure, air temperature. It is important to recall that inside of RLV the fuel play a cooling role [40] and surface can be covered with high thermal resistance materials [41].

3.7 MATLAB Simulink model

3.7.1 Presentation

This part aims to understand the interest of using the attack angle to increase the drag force, and thus the kinetic energy consumed. All the energy consumed by air friction will be less energy supplied to the motors to decrease the speed before landing. This energy has a weight, because the fuel used at the end, has to be transported during the whole flight, a decrease in volumes is needed for cost savings.

By application of the equations of the structure (*3.3 Equation of trajectory control*), the mechanical model can be built.

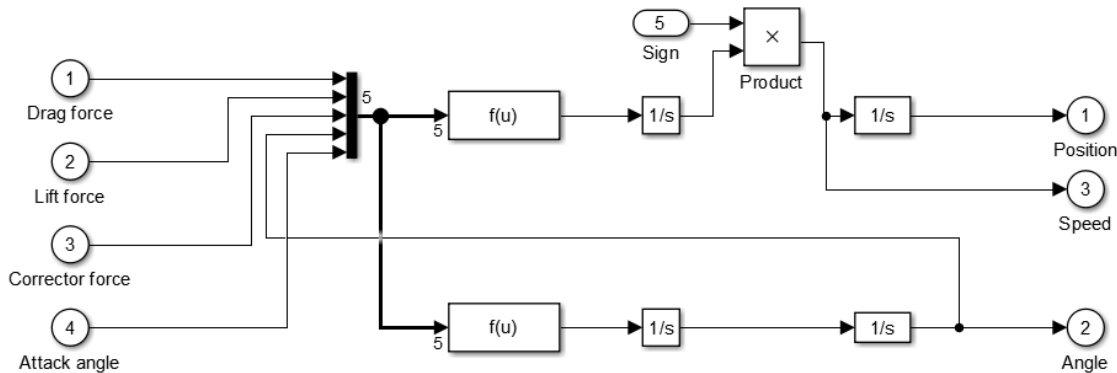


Figure 3.18 Mechanical model of RLV during reentry phase, force on x axis

The correction forces are provided by the trajectory controllers. From the top of the RLV, this force controls the angle of the RLV and therefore the angle of attack. In this case study, all parameters are interdependent, all parameters are inside a closed loop. The starting point inside the loop is the angle of attack necessary to know the aerodynamic forces. This angle of attack is a function of the rocket angle and speeds. In reality, there is only one angle of attack. The real problem will be separate into two 2D problems, they will be combined later.

To assess the value of this angle of attack, two positions case have been taken into account as presented in *Figure 3.19*. Two cases have to be considered, for that the absolute value will

be calculated. However, to know the sign of the angle, a sign parameter is created, visible in *Figure 3.18*.

$$\alpha_{roll} = |\theta - \arctan\left(\frac{V_x}{V_y}\right)| \quad (3.22)$$

$$\alpha_{pitch} = |\theta - \arctan\left(\frac{V_z}{V_y}\right)| \quad (3.23)$$

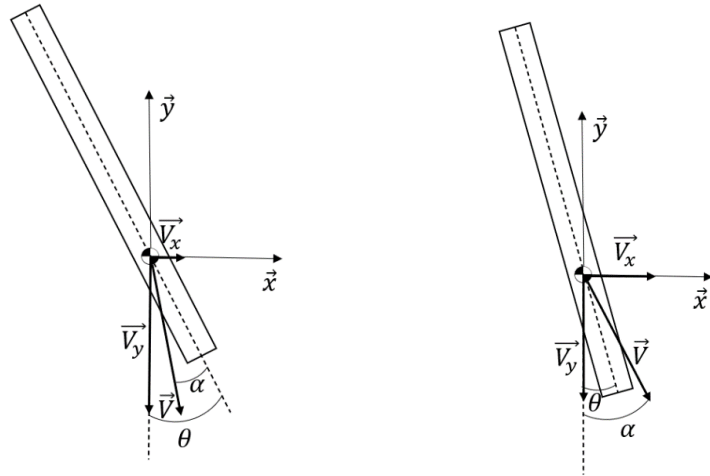


Figure 3.19 Representation of attack angle

Given the values of the attack angles, it is possible to calculate the drag and lift force, by the application of the ratio formulas described previously. Even if this problem is divided in two 2D problems, the forces exerted on the y axis must take into account the 3D characteristics of this model. The link between the two 2D dimensions model and the 3D model has to be investigated.

The link between these three angles are detailed as follows and presented in *Figure 3.20*:

$$a = n * \tan(pitch) \quad (3.24)$$

$$b = n * \tan(roll) \quad (3.25)$$

$$c = \sqrt{a^2 + b^2} \quad (3.26)$$

$$\alpha = \arctan(c/n) \quad (3.27)$$

$$\alpha = \arctan\left(\frac{1}{n} * \sqrt{n^2 \cdot \tan^2(pitch) + n^2 \cdot \tan^2(roll)}\right) \quad (3.28)$$

$$\alpha = \arctan(\sqrt{\tan^2(pitch) + \tan^2(roll)}) \quad (3.29)$$

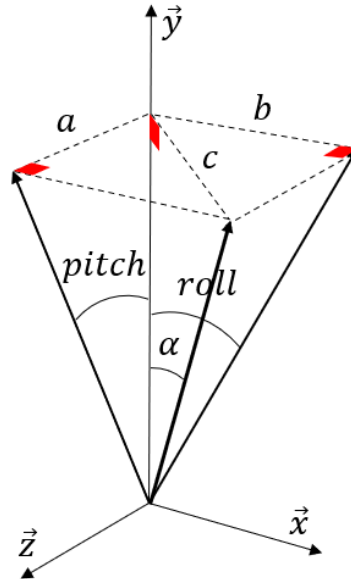


Figure 3.20 Attack Angle 3D relation

Comment

The attack angle detailed on the previous page is named pitch or roll function of each 2D dimension model. Here the attack angle noted α is the attack angle in 3D.

Knowing the evolution of the air density function of the altitude, the function links the attack angle, the rocket angle and the ratio of aerodynamic forces. The model can be developed and run.

3.7.2 Result

Our model of study is an RLV with the Falcon 9 shape to use the ratio's theory developed previously, however the dimensions will be proportionally smaller.

RLV settings:

- Masse: 400 kg
- Length: 7 m
- Radius: 0.29 m
- Inertia: 1650 kg.m²

These values are selected to keep the same density than Falcon 9.

The settings of these experiments:

- The initial altitude is 40 km
- The initial speed is equal to zero
- Overlooks the archimedean thrust
- The wind is considered equal to zero

List of experiments

- Free fall without atmosphere
- Free fall with atmosphere
- Control 2D angle of attack
- Control 2D angle of attack with sinusoid command
- Control 2D angle of attack with gate command
- Control 3D angle of attack with helical effect

Result of experiment:

- Arrival time or ratio time
- Distance between RLV and the vertical point

3.7.2.1 Free fall without atmosphere

This free fall is here to validate the model. By system application of Newton 2nd law, it is possible to know the time took by the RLV to go down the 40 km.

$$t = \sqrt{\frac{2*h}{g}} = \sqrt{\frac{2*40000}{9.81}} = 90.3 \text{ s} \quad (3.30)$$

This calculation validates the value found with this model.

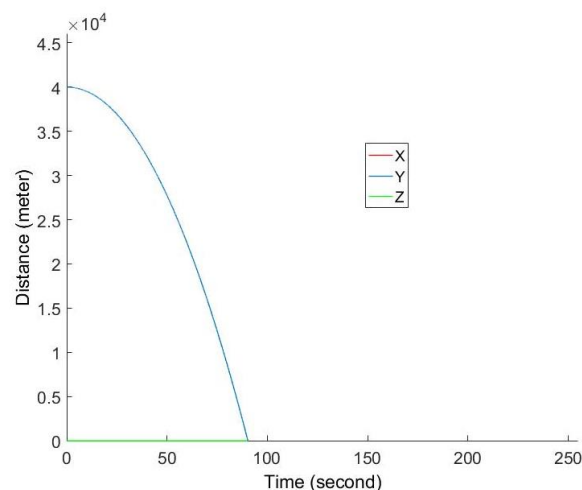


Figure 3.21 Free fall without atmosphere

3.7.2.2 Free fall with atmosphere

For this experiment, the return time of the rocket will be realistic. That will be the reference time. For the next part, this reference time will be useful to develop the time ratio curve. The reference is 145.57 seconds as shown in the next figure. The ratio expression is explained below.

$$Ratio_{time} = \frac{Time_{touchdown}(attack\ angle)}{Time_{touchdown_0}} \quad (3.31)$$

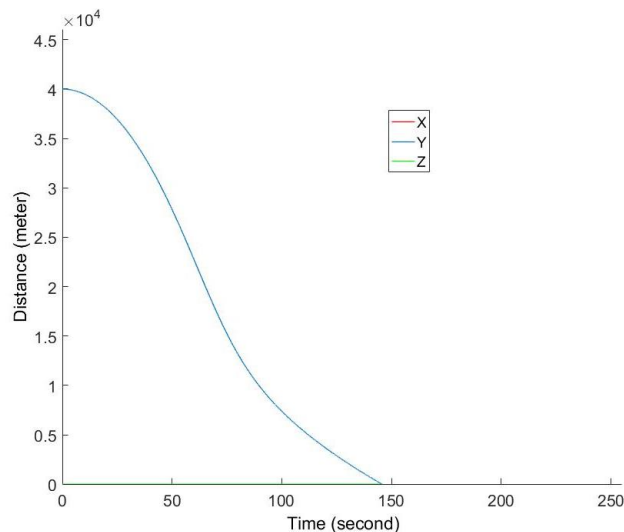


Figure 3.22 Free fall with atmosphere

3.7.2.3 Control 2D angle of attack

For these tests, the attack angle is controlling, in a simple way. One value is selected at the beginning and stays the same during the whole reentry phase. These tests aim is to find the best value of the attack angle. The following curve shows the evolution of the time ratio function of this angle. The inflection point of the curve is around the 30° , this value is selected as the best attack angle.

As explained in part 3.2 and shown in *Figure 3.7*, 30° of attack angle gives a strong lift force, equivalent to the drag for this attack angle. Thus, the RLV should have a large displacement along the tilt axis. The following figure presents the displacement on the three axes, that confirm the prediction.

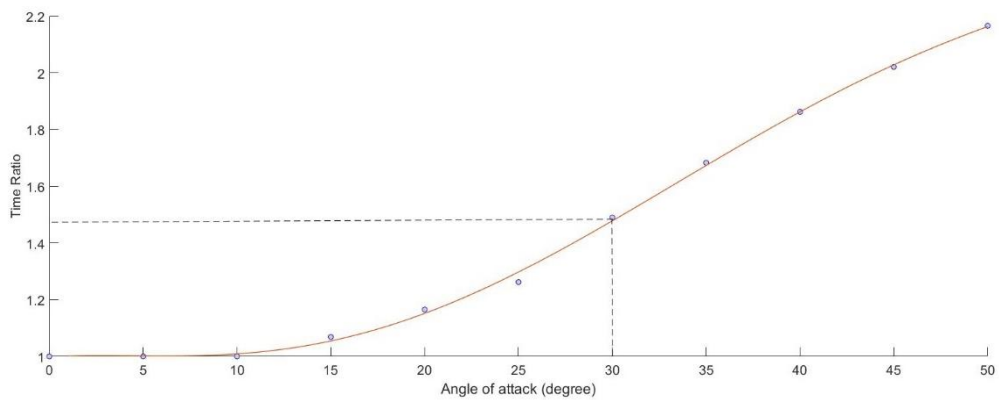


Figure 3.23 Time Ratio curve function of angle attack

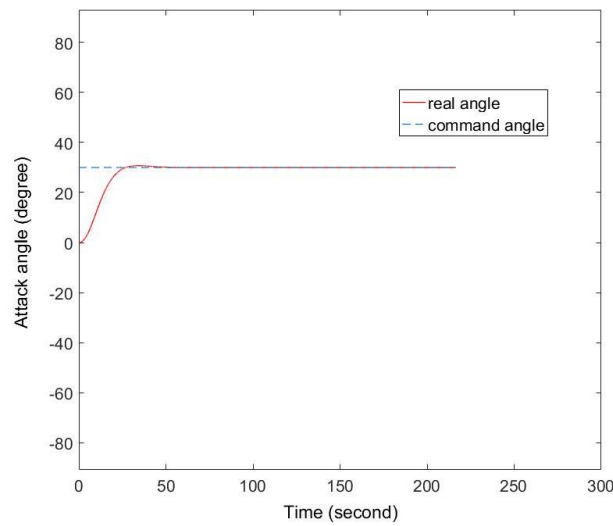


Figure 3.24 Reentry trajectory for 30° of attack angle

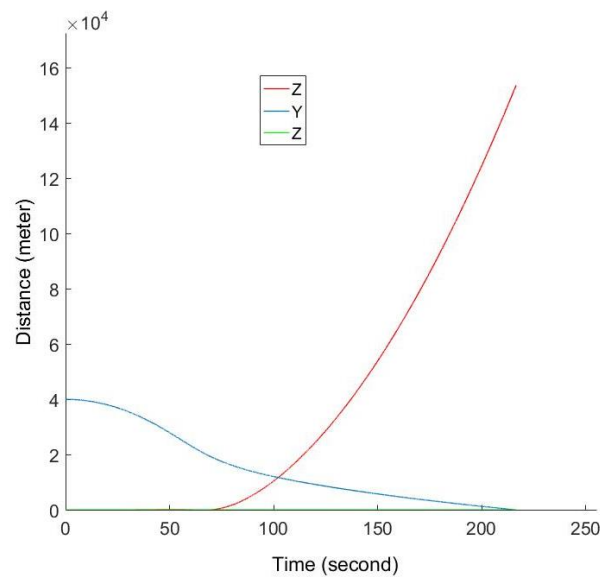


Figure 3.25 Angle attack for 30° of command

For better understanding each figure of displacement will be joined to the attack angle figure.

3.7.2.4 Control 2D angle of attack with sinusoid command

The ratio of the previous test was around 1.5, which means the RLV will take 50 % more time to reach the ground, thus energy is consumed thanks to aerodynamic forces. Unfortunately, the displacement on the horizontal axis is very important. This part and the next one will present other ways to use the aerodynamic effect while touching the landing zone at the end.

The attack angle will be command via a sinusoidal function to keep a “vertical” trajectory.

$$\alpha_{command}(t) = 30 * \cos\left(\frac{2\pi t}{53}\right) \quad (3.32)$$

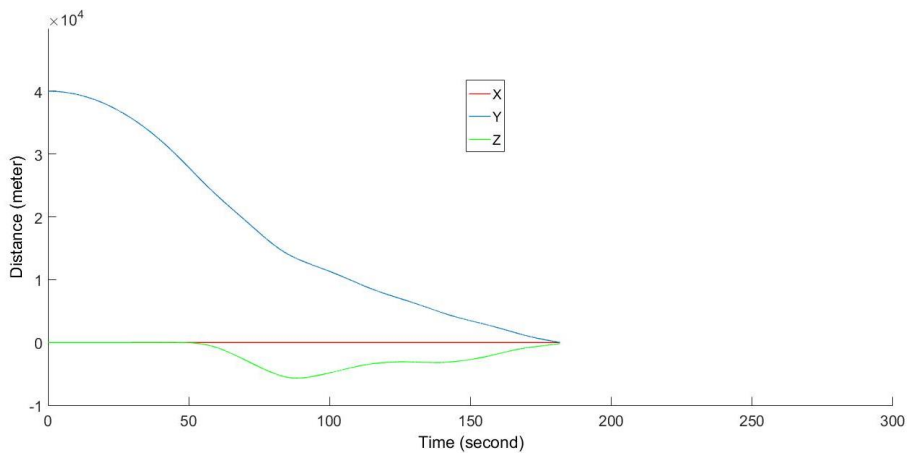


Figure 3.26 Reentry trajectory sinusoid command

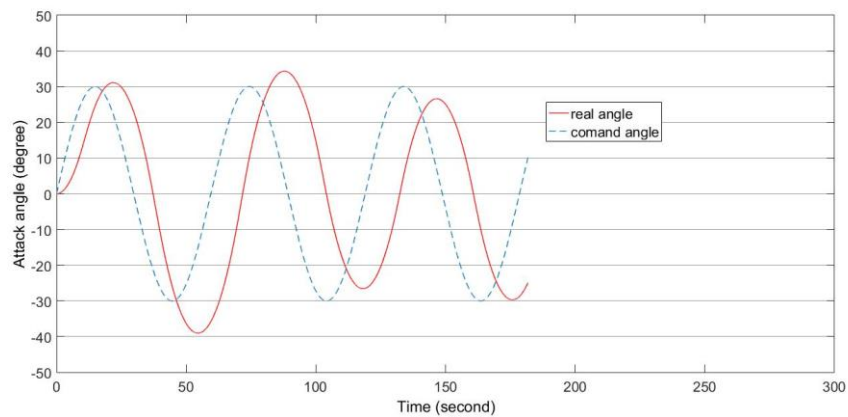


Figure 3.27 Angle attack sinusoid command

For this setting the arrival time is 181 seconds and the delta position is null.

3.7.2.5 Control 2D angle of attack with gate command

The attack angle will be command via a gate function to keep a “vertical” trajectory.

$$\alpha_{command}(t) = \begin{cases} 30 & \text{if } N * 40 < t < (N + 1) * 40 \\ -30 & \text{if } (N + 1) * 40 < t < (N + 2) * 40 \end{cases} \quad (3.33)$$

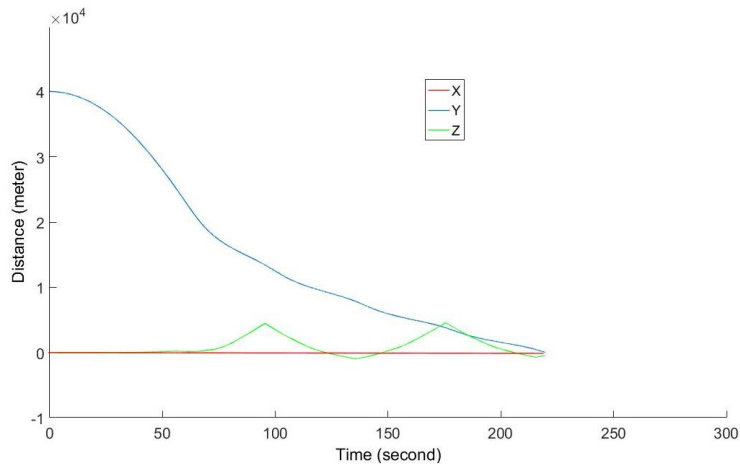


Figure 3.28 Reentry trajectory for small gate command

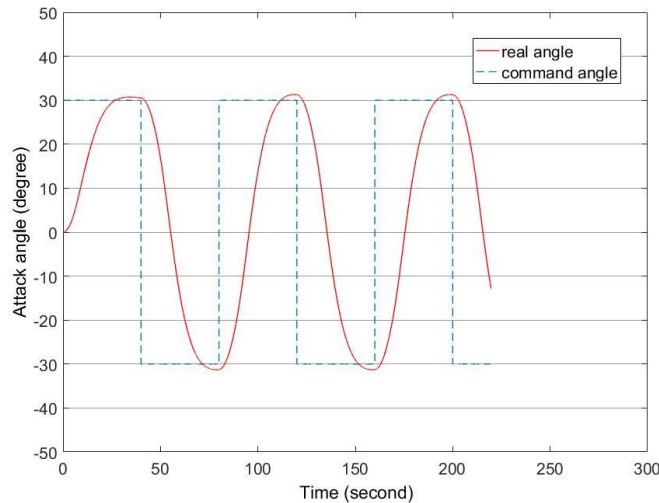


Figure 3.29 Angle attack for small gate command

For this setting the arrival time is 219 seconds and the delta position is null.

The gate impulsion command can be applied for a long period, the arrival should be better. However, the RLV will no keep a “vertical” trajectory. Check by calculation on the next experiment.

$$\alpha_{command}(t) = \begin{cases} 30 & \text{if } N * 152 < t < (N + 1) * 152 \\ -30 & \text{if } (N + 1) * 152 < t < (N + 2) * 152 \end{cases} \quad (3.34)$$

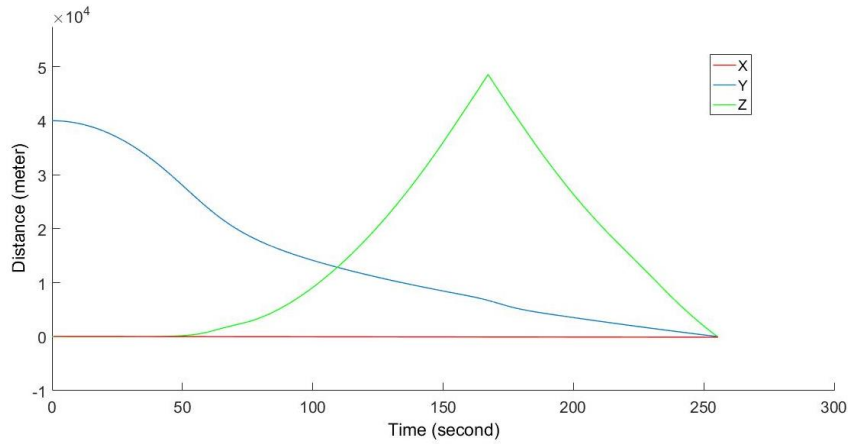


Figure 3.30 Reentry trajectory for large gate command

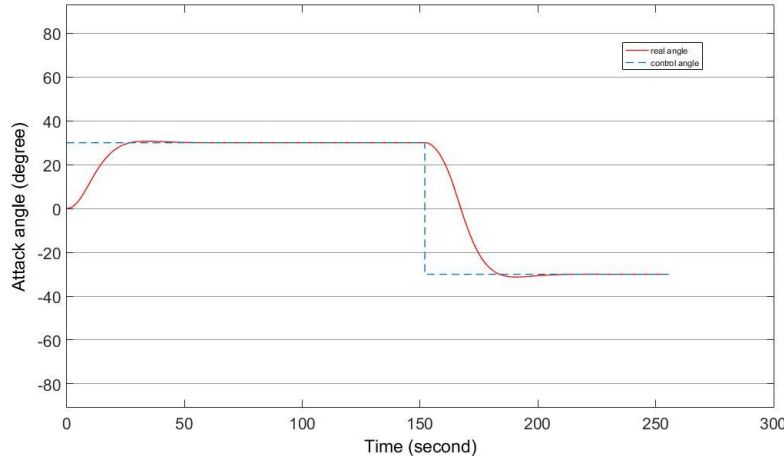


Figure 3.31 Angle attack for large gate command

For this setting the arrival time is 255 seconds, and the delta position is null.

One new requirement has to be added, it is the maximum delta with the vertical line. In the last experiment the RLV goes far to the vertical line before come back. However, this method can be used for travel to reach the landing zone if it is not on the vertical.

3.7.2.6 Control 3D angle of attack with helical effect

Each idea presented above is done in 2 dimensions. The goal is to find a solution, in 3 dimensions. Which takes into account all the requirements and which has a longer reentry time,

therefore a better use of the aerodynamic forces. For this, a natural element was inspiring: maple leaves. When they fall, they use the rotation around them to reduce the vertical speed, so they stay in the air longer and are more likely to be caught by the wind to move away. Following this natural inspiration, an experiment is conducted.

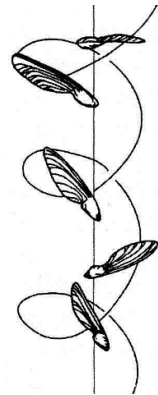


Figure 3.32 Maple leaves trajectory

The attack angle will be command via two sinusoidal function, to creat a helicoidal trajectory around the “vertical” line.

$$\alpha_{command/pitch}(t) = 30 * \cos\left(\frac{2\pi t}{50}\right) \quad (3.35)$$

$$\alpha_{command/roll}(t) = 30 * \sin\left(\frac{2\pi t}{50}\right) \quad (3.36)$$

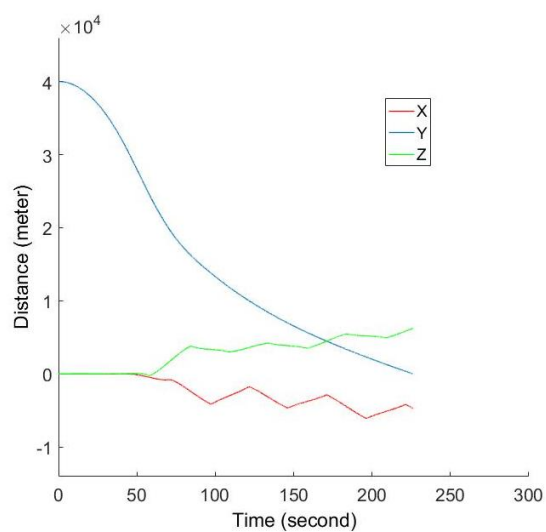


Figure 3.33 Reentry trajectory for 3D cercle command

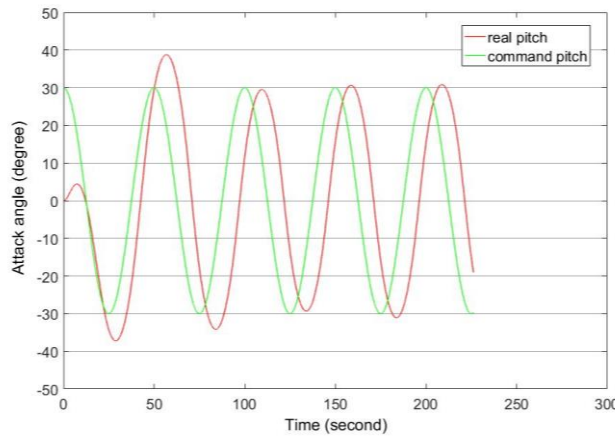


Figure 3.34 Angle attack (pitch) for 3D cercle command

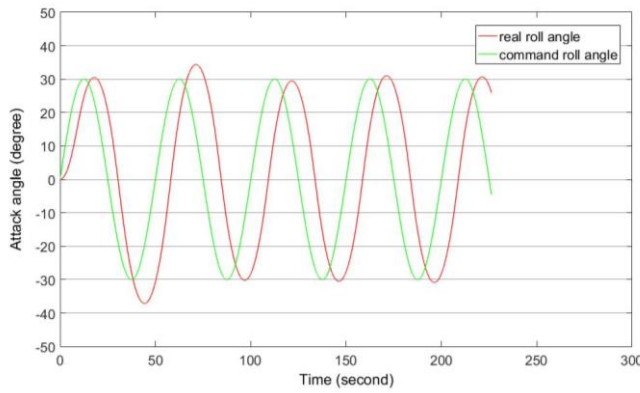


Figure 3.35 Angle attack (roll) for 3D cercle command

For this setting the arrival time is 226 seconds and the delta position is around 10 km.

3.7.2.7 Comparaison of experiment

For a better understanding of the action of the angle of attack on the RLV's re-entry trajectory, a graphical report bar is constructed.

The three values compared are:

- travel time
- accuracy on the landing zone
- maximum distance during the flight compared to the vertical line.

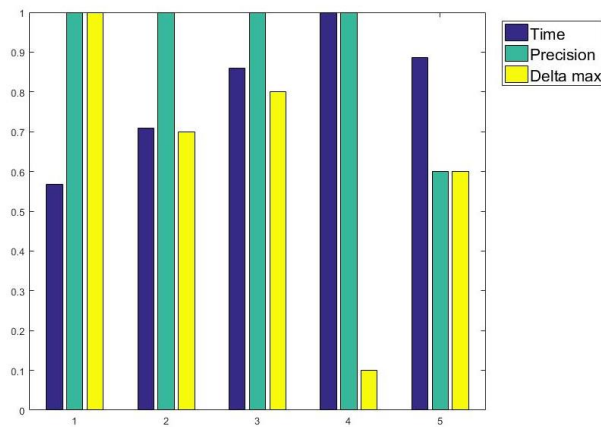


Figure 3.36 Graph of comparisons of the different trajectories design

In the graph view, the control 3 and 5 are the best option, they will be used for the last global trajectory control present on the next step.

3.8 Conclusion

These experiments confirmed that the control of the attack angle can manage the trajectory of the RLV. It is shown also the possibility to keep a trajectory line and around this one takes different angles for the RLV, thus change the aerodynamic effects.

To finished this chapter one potential trajectory of RLV is presented, reusing the attack angle control presented previously.

The idea of landing trajectory, firstly the RLV comes on the top of the landing zone, secondly the RLV turns around its inertia center, with helicoid trajectory. The helicoid decreasing to arrive at a zero, then is the last step, the engines control the touch down as a vector rocket, this last step is developed in the next chapter.

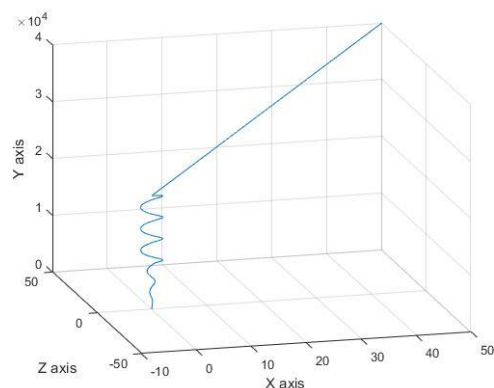


Figure 3.37 Idea of RLV reentry trajectory

Chapter 4 End phase control design

4.1 Introduction

This is probably the most important landing process. At this stage, it is too late to correct trajectory errors. That is why the last 500 meters have to be precisely controlled. The velocity of the RLV is very low compared to the previous phase and here the aerodynamic force can be overlooked. From that point, flight considerations change, the main focus is no longer energy consumption but safety. During the phase of landing the rocket must keep a perfect vertical position.



Figure 4.1 The two-lateral booster of the falcon heavy just before the touch down in Texas

For this model, the rocket will be considered as a solid pipe of constant density. About the propulsion the choice will be a vector force at the bottom of the pipe. The physical problem is close to the inverse pendulum problem, with only the propulsion to control the position of the rocket. However, the usual reverse pendulum is only in 2 dimensions, for this model the RLV must be able to adjust itself to the horizontal position to set the last meters of the reentry phase in 3 dimensions.

For this part, will present the development of the software controlling the RLV during this phase. The physical model will be based on the inverted pendulum but adapted to the case studied. Then, a Simulink model will be built and a virtual world will be created to present a good interface, the "VR Sink" [42] module proposed by Simulink will be used.

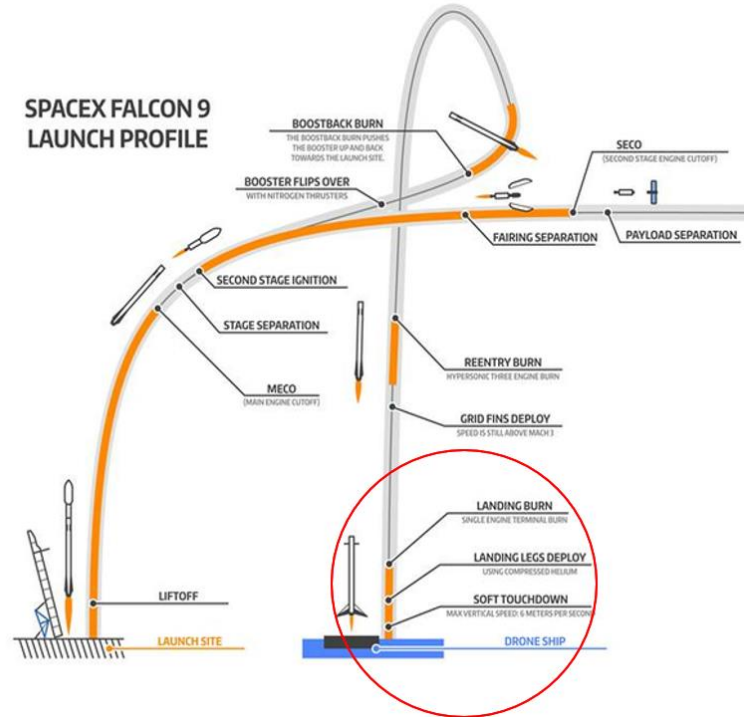


Figure 4.2 Graphic representation of the trajectory of the booster of the falcon 9

4.2 Inversed pendulum model

The length of rocket noted: L

The masse of rocket noted: m

The gravity acceleration noted: g = 9.81 m/s

The angle between vertical axis and rocket axis noted: φ

The inertial of rocket around side axis noted:

$$I = \frac{m}{4} (R^2 + \frac{h^2}{3}) \quad (4.1)$$

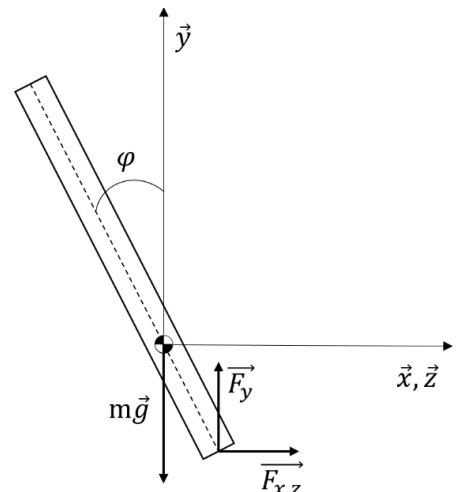


Figure 4.3 RLV model system

(1) Equations of the structure

$$m \cdot \ddot{x}_G = Fx \quad (4.2)$$

$$m \cdot \ddot{y}_G = Fy - m \cdot g \quad (4.3)$$

$$I \cdot \ddot{\varphi} = (\frac{L}{2}) \cdot \cos(\varphi) \cdot Fx + (\frac{L}{2}) \cdot \sin(\varphi) \cdot Fy \quad (4.4)$$

(2) Bond equations

$$\ddot{x}_G = \ddot{x} - \left(\frac{L}{2}\right) \ddot{\varphi} \cdot \cos(\varphi) + \left(\frac{L}{2}\right) \dot{\varphi}^2 \cdot \sin(\varphi) \quad (4.5)$$

$$\ddot{y}_G = \ddot{y} - \left(\frac{L}{2}\right) \ddot{\varphi} \cdot \sin(\varphi) - \left(\frac{L}{2}\right) \dot{\varphi}^2 \cdot \cos(\varphi) \quad (4.6)$$

$$Fx = F \cdot \sin(\alpha) \quad (4.7)$$

$$Fy = F \cdot \cos(\alpha) \quad (4.8)$$

With α the engine angle $\alpha = 0^\circ$ when trust engine is on the vertical axis

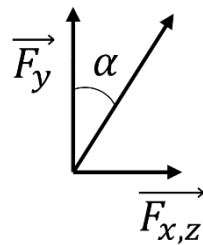


Figure 4.4 Coordinate system of engine force

$$Fx = m \cdot \ddot{x} - m \cdot \frac{L}{2} \cdot \ddot{\varphi} \cdot \cos(\varphi) + m \cdot \left(\frac{L}{2}\right) \dot{\varphi}^2 \cdot \sin(\varphi) \quad (4.9)$$

$$\boxed{m \cdot \ddot{x} = Fx + m \cdot \frac{L}{2} \cdot (\ddot{\varphi} \cdot \cos(\varphi) - \dot{\varphi}^2 \cdot \sin(\varphi))} \quad (4.10)$$

$$Fy = m \cdot g + m \cdot \ddot{y} - m \cdot \frac{L}{2} \cdot \ddot{\varphi} \cdot \cos(\varphi) + m \cdot \left(\frac{L}{2}\right) \dot{\varphi}^2 \cdot \sin(\varphi) \quad (4.11)$$

$$\boxed{m \cdot \ddot{y} = -Fy - m \cdot g + m \cdot \frac{L}{2} \cdot \ddot{\varphi} \cdot \cos(\varphi) - m \cdot \left(\frac{L}{2}\right) \dot{\varphi}^2 \cdot \sin(\varphi)} \quad (4.12)$$

$$I \cdot \ddot{\varphi} = \left(\frac{L}{2}\right) \cdot \cos(\varphi) \cdot (m \cdot \ddot{x} - m \cdot \frac{L}{2} \cdot \ddot{\varphi} \cdot \cos(\varphi) + m \cdot \left(\frac{L}{2}\right) \cdot \dot{\varphi}^2 \cdot \sin(\varphi)) \quad (4.13)$$

$$+ \left(\frac{L}{2}\right) \cdot \sin(\varphi) \cdot (m \cdot g - m \cdot \frac{L}{2} \cdot \ddot{\varphi} \cdot \cos(\varphi) + m \cdot \left(\frac{L}{2}\right) \cdot \dot{\varphi}^2 \cdot \sin(\varphi)) \quad (4.14)$$

$$\boxed{\left(m \cdot \left(\frac{L}{2}\right)^2 + I\right) \cdot \ddot{\varphi} = m \cdot \left(\frac{L}{2}\right) \cdot (\ddot{x} \cdot \cos(\varphi) + g \cdot \sin(\varphi))} \quad (4.15)$$

Thanks to the previous equations of \ddot{x} and $\ddot{\varphi}$, a Simulink bloc system can be built. The block relation is named $f(u)$ on the *Figure 4.5*.

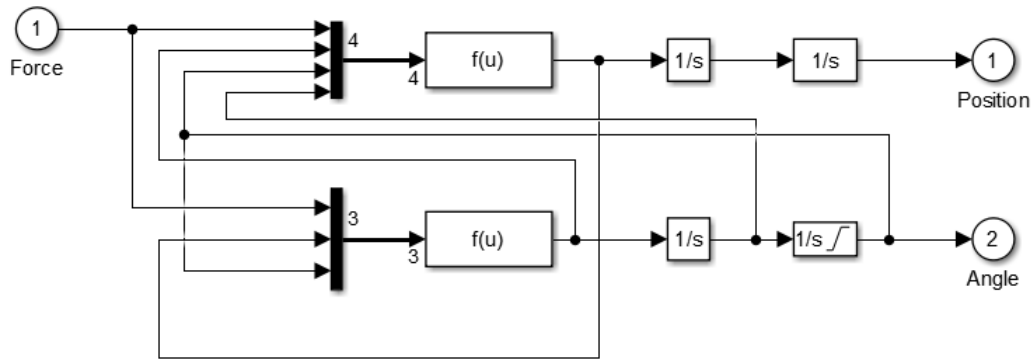


Figure 4.5 Equation of balance system from Newton laws

4.3 3-dimensional model

Figure 4.6 presents the solution to pass from 2 Dimensions problem to 3 Dimensions. Thus, this problem is divided into two different inverted pendulums in two plans; one perpendicular to x axis and one perpendicular to z axis.

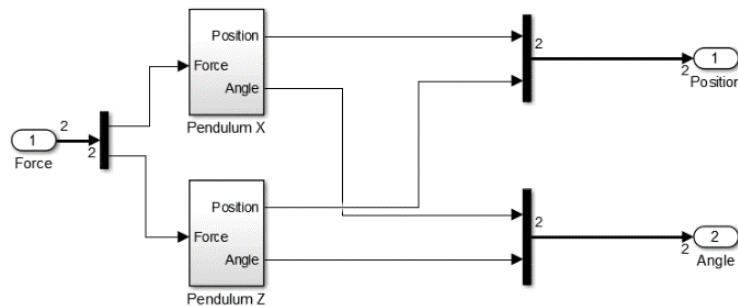


Figure 4.6 From 2D to 3D system

4.4 PID control

4.4.1 Presentation

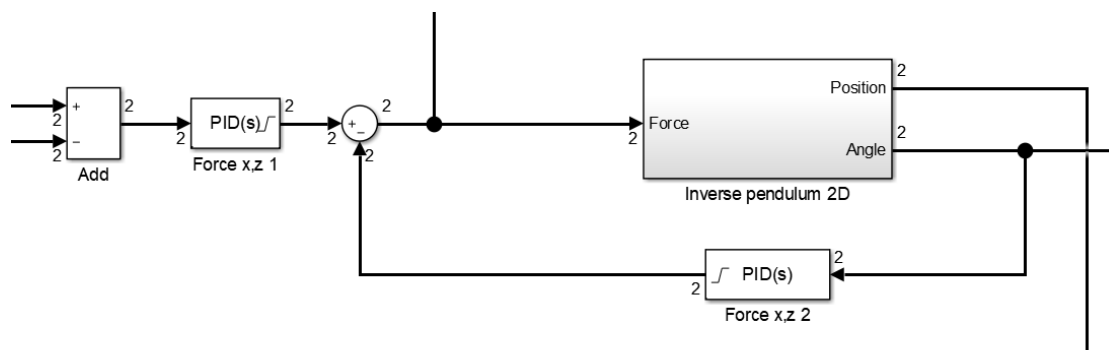


Figure 4.7 Double loop PID, angle stability and position control

Our system is highly unstable due to the non-linearity of the problem, that is why in the return loop, a PID corrector [43] has to be added to take into account the balance effect.

Thus, two PID controllers have to be adjusted. Unfortunately, MATLAB cannot automatically adjust due to this non-linearity. Sometimes for some non-linear system the solution can be to divide the system in two parts to get two linear systems. However, in this case is impossible to separate the problem in two PID system managed one by one, that have to be like shown on the *Figure n°4.7*.

Important notice: the value of PID depends on physical equation and for that reason the value of PID will be quite different between different rockets. Nevertheless, a system available for every rocket will be preferable.

To simplify the obtention of PID value the PID on the position will be only PD controller. That mean 5 parameters have to be adjusted in function of the length, masse and inertia of rocket and the gravity acceleration.

$$P + I \frac{1}{s} + D \frac{N}{1+N \frac{1}{s}} \quad (4.16)$$

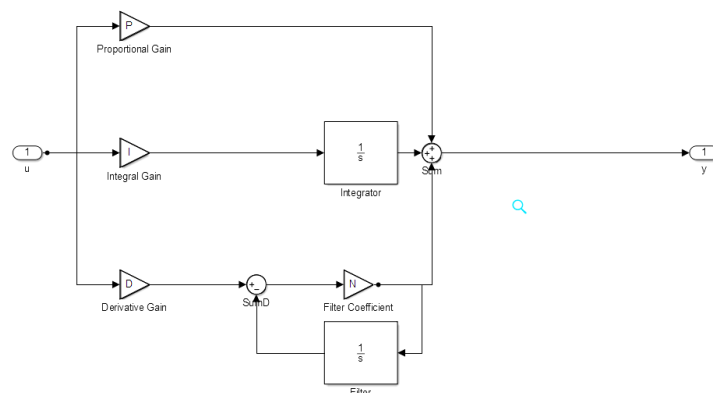


Figure 4.8 PID blocks model

To be able to find the good PID coefficients, it is necessary to know how these coefficients affect the system answer. *Table 4.1* just below is a good help to estimate the system answer function PID coefficients.

Table 4.1 PID explication

	Precision	Speed	Stability
Proportional	↑	↑	↓
Integral	↑	↓	↓
Derivate	↓	↑	↑

Before setting up a graphic methodology to get an automatic PID control, the engine power has to be taken into consideration. Indeed, the engine power depends directly to the masse of the RLV by choice this ratio will be equal to 2. As for an example if the masse of the RLV is equal to 1kg the maximum thrust of engine will be 2 kg. This ratio will be placed in the loop on the back of the forces value and used as proportional coefficient, (see on the *Figure 4.11*).

After several tests with different values of the PID coefficients, it is observed that the values of the PD coefficients used for distance control can be the same for different rocket dimensions. It is because the distance between the landing zone and the rocket does not depend on the dimension of the RLV. Thus, only three variables (P, I, and D) for the balance control have to change the function of RLV dimensions.

4.4.2 PID curves control

This method aims to assess the value of each coefficient of PID which controls the balance of RLV, each coefficient will follow one curve. This graphical solution has been based on experimental trials.

The selected shape is a cylinder and the center of inertia is placed in the middle. Also, the relation between masse and dimension is constant, according to the Falcon 9 booster properties. The only variable is the length of the RLV.

The density will be kept constant with the value: $\rho_{falcon9} = 211.66 \text{ kg.m}^{-3}$

$$\text{Mass} = \rho_{falcon9} * \pi * r^2 * \text{Length} \quad (4.17)$$

$$\text{Radius} = \text{Length}/23,8 \quad (4.18)$$

To plot the control PID calibration curves many tests have been done with different lengths, as shown in the following graph:

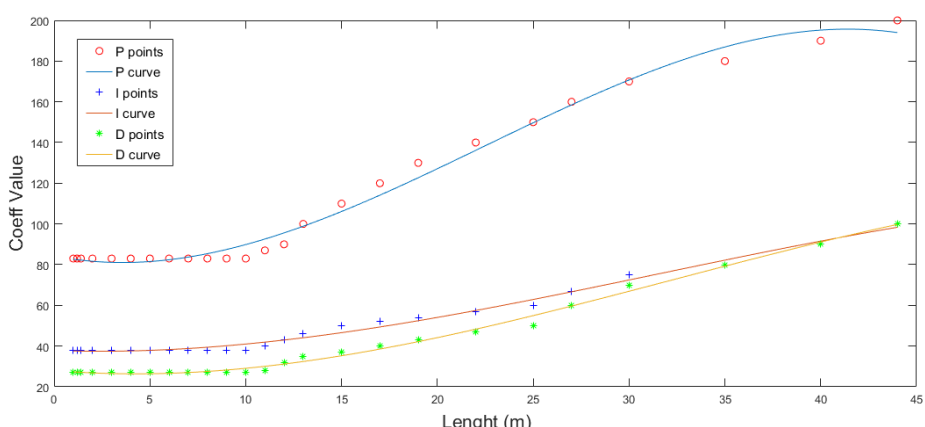


Figure 4.9 Curve of PID coefficient function of length of RLV

4.4.3 Equation of PID coefficient

The equations are found by the MATLAB function Polyval [39], the curves of these ones are presented on the previous graphics, *Figure 3.6*.

$$P(L) = -0.0042 * L^3 + 0.2854 * L^2 - 1.8742 * L + 84.3006 \quad (4.18)$$

$$I(L) = -0.0008 * L^3 + 0.0727 * L^2 - 0.3354 * L + 37.8584 \quad (4.19)$$

$$D(L) = -0.0011 * L^3 + 0.1017 * L^2 - 0.8084 * L + 28.0509 \quad (4.20)$$

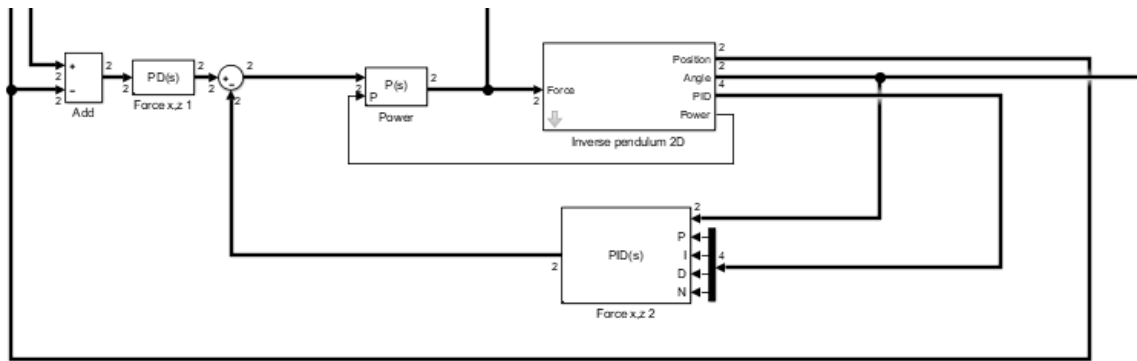


Figure 4.10 Double PID loop with angle PID autonomous control and powerful adaptation

This type of control with variation of the control coefficient can be useful to manage the evolution of the weight during the flight, according to the fuel consumption.

4.5 Altitude control

4.5.1 Presentation

The last parameter to control is the altitude. The physical equations have been detailed on the previous part *4.3 Inversed pendulum model*, recapped below.

$$m \cdot \ddot{y}_G = Fy - m \cdot g \quad (4.21)$$

$$Fy = F \cdot \cos(\alpha) \quad (4.22)$$

$$m \cdot \ddot{y}_G = F \cdot \cos(\alpha) - m \cdot g \quad (4.23)$$

If previously the simulation was 2D for the horizontal translation, with two inverted pendulum models, now for the vertical axis (y) it is necessary to back in 3D. Thus, to know the value of the engine angle noted α . This angle is function of the two angles pitch and roll of the engine. *Figure 3.19* was detailed in the previous chapter.

$$\alpha = \arctan(\sqrt{\tan^2(pitch) + \tan^2(roll)}) \quad (4.24)$$

The angle formula set up; the Simulink model can be fine tuned. This time, the control system is linear, so it is easier to find the right PID values, and these will be available for a larger range of rockets (mass, inertia, length). In addition, MATLAB is able to find the best one for you by calculation thanks to the linearity of the problem.

4.5.2 MATLAB Simulink model

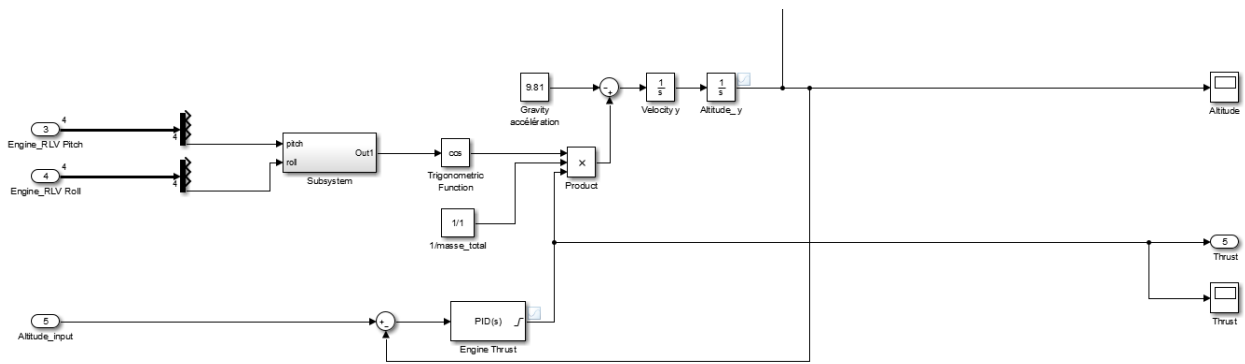


Figure 4.11 Simple loop PID altitude control

To validate the right comportment of the rocket controlled by this PID loop, two tests must be successful: the rocket answers to a gate (increase, decrease altitude), the rocket answers to the horizontal movement, so tilt of vertical axis.

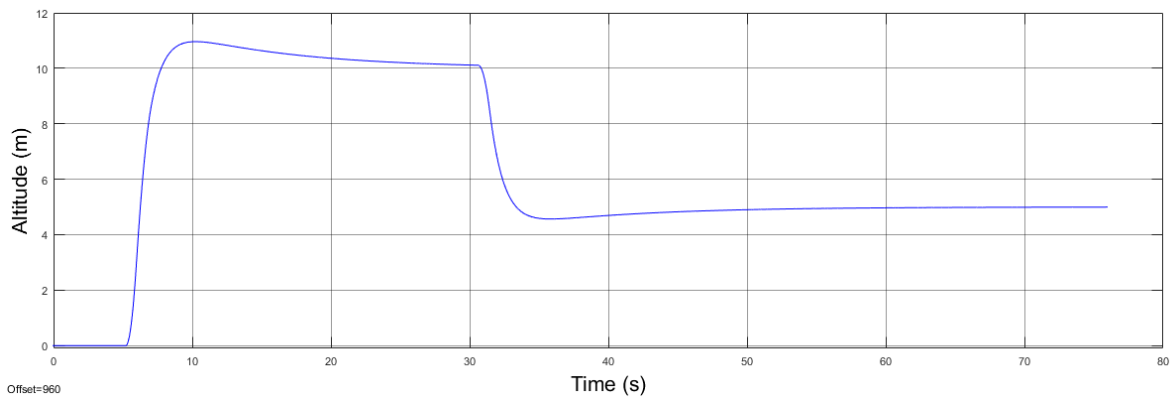
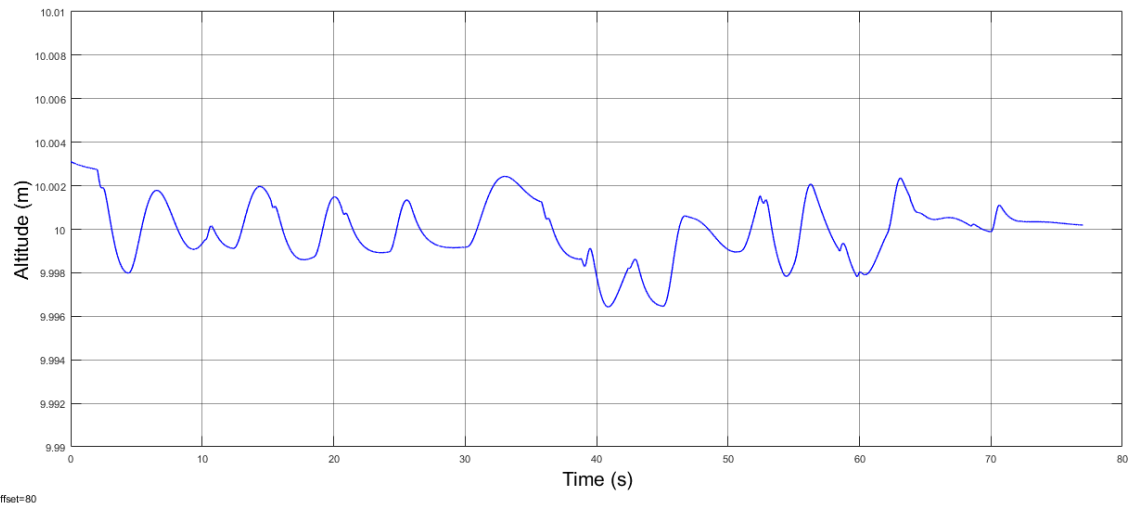


Figure 4.12 Altitude of rocket subject to an altitude command + 10m and - 5m



4.6 Control parameter

One last point must be solved before executing the model. By taking the thrust with two components for the pendulums inversed, and knowing now the force necessary to maintain a pilot altitude, it is possible to determine the roll and pitch angle.

$$Fx = F \cdot \sin(\alpha) \quad (4.25)$$

$$Fy = F \cdot \cos(\alpha) \quad (4.26)$$

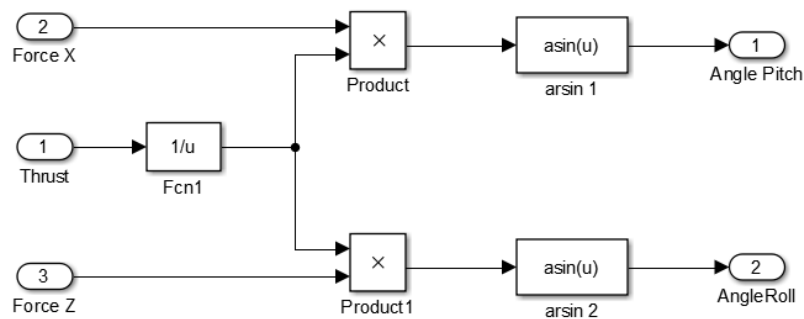


Figure 4.14 Angle value of real thrust of the engine

4.7 Global MATLAB Simulink

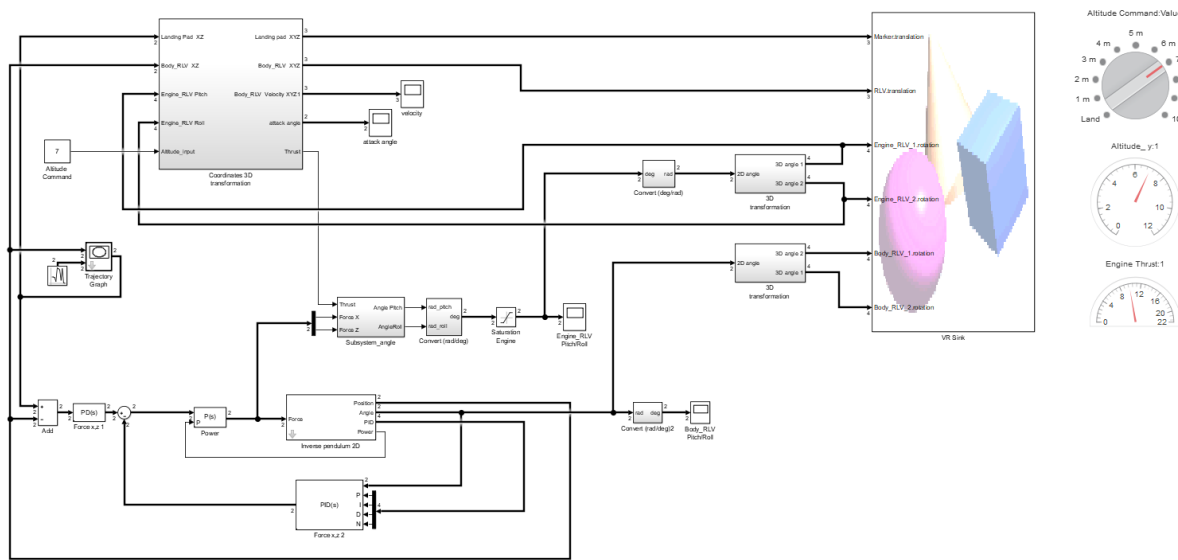


Figure 4.15 Full Simulink model of vector rocket control (Annex 4.1)

4.8 3D Virtual world

The aim of this virtual world is to give an appropriate interface for this model, as well as an easy way to understand and find the right PID coefficient value. The modifiable settings are in 3 dimensions (x, y, z). The x and z value are managed by the position of the red point on the landing pad (grey area) modifiable by a simple mouse click on it. The altitude (y) is selectable meter by meter.

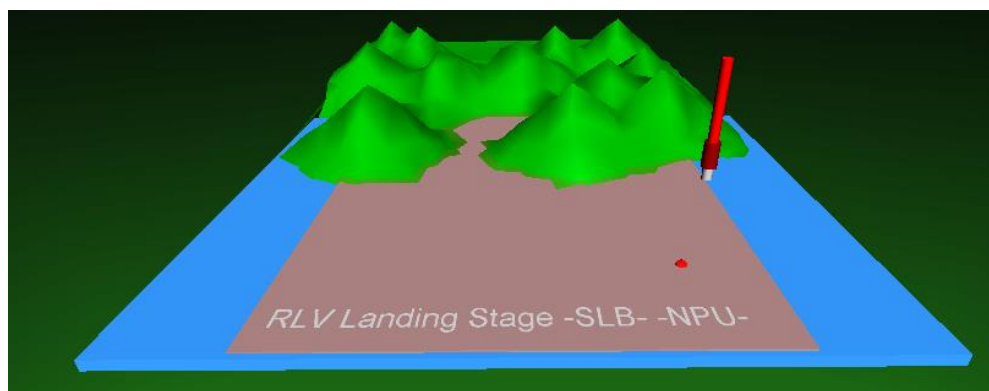


Figure 4.16 3D Virtual World

4.9 Result of simulation

One spectral photo of the horizontal translation from left to right is illustrated below. On the next page four graphics show the movement of the RLV: Angle view (body and engine), Velocity and X, Z position.

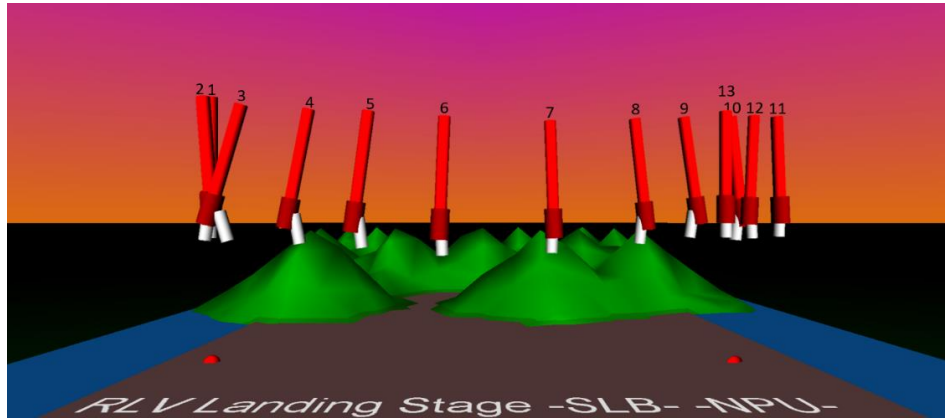


Figure 4.17 RLV translation on 3D Virtual World

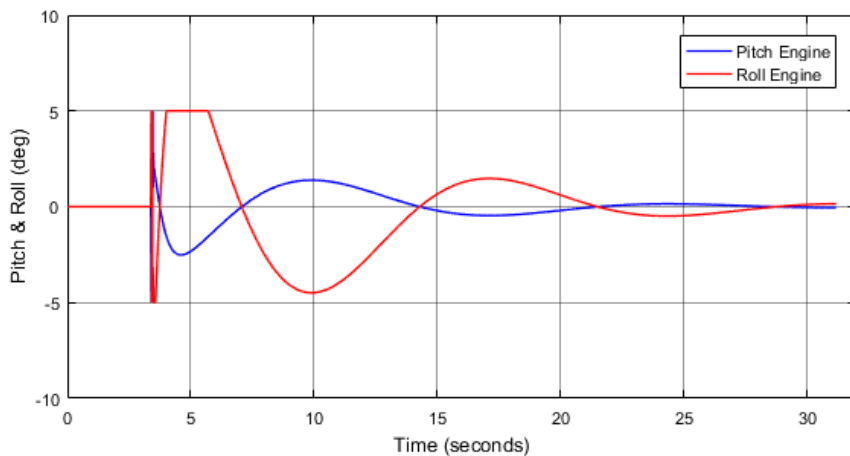


Figure 4.18 Pitch and Roll of Engine

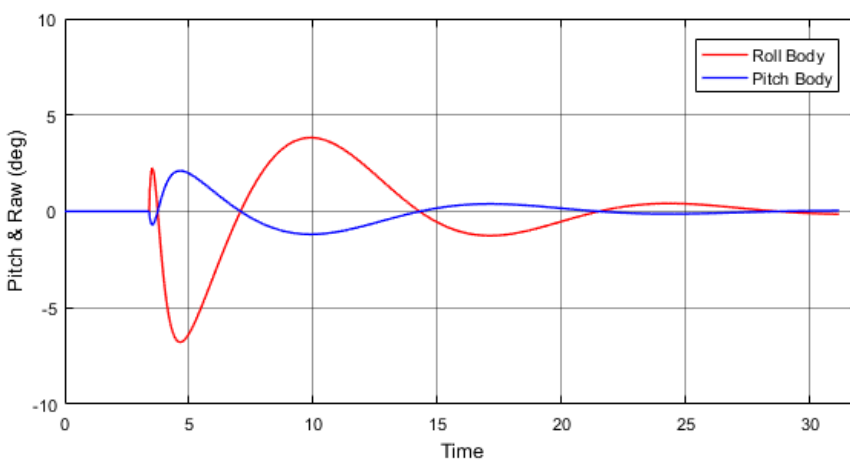


Figure 4.19 Pitch and Roll of Body

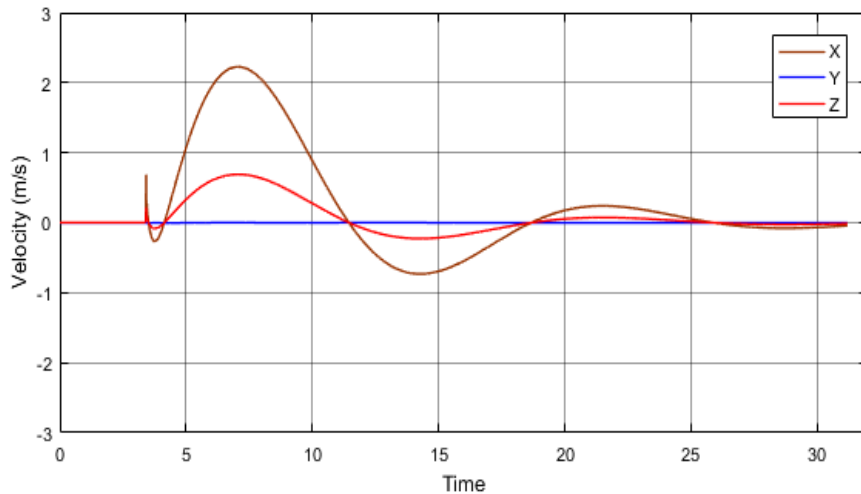


Figure 4.20 Pitch and Roll of Body

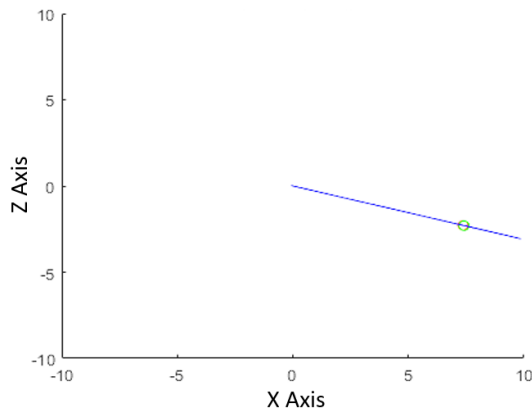


Figure 4.21 XZ Graph trajectory of RLV

Remark

To reflect reality as carefully as possible, some mechanical considerations have to be taken into account. The first one is the limit of the angle value of the rocket to be sure to keep control, with a maximum at 10° compared to the vertical axis. The second one is the angle of the engine that has been selected with max value of 5° (see in the *Figure 4.18*).

4.10 Conclusion

This study showed the high instability of the vector rocket. However, it showed also the possibility of controlling it by using PID. Another very promising way will be controlling this instability by using AI, by learning.

The system control can be suitable for many applications and not only the landing of the booster, even if today it is the major commercial project. Others interesting projects can be controlled with the same method, as witnessed the Space X Starhopper [44], which are planned to be used to reach the Martian surface.



Figure 4.22 Space X Starhopper during flight test in Texa

Chapter 5 Validation of end phase control

5.1 Introduction

Aerospace is a world where the gap between simulation and reality is huge. In the simulation we had already touched the surface of Mars and even by many times but in reality, no dedicated spacecraft has been built yet. At the opposite of all other parts of this thesis, Chapter 5 presents RLV real-time tests. We've built several models of RLV, for which of course the size was very small compared to the huge size of spatial structures in reality. However, it was important for me to build it myself to realize technical issues that aerospace engineers have been facing or years. For this part, the compiled information described in Chapter 4 has been very helpful for the choices that have been made to select the best RLV model.

The size will be comparable to the huge Falcon 9 of Space X many times presented in this thesis. The propulsion will not be provided by the thermic engine but via an electric one, connected to the propeller system. From now, this RLV is a vector rocket, all issues are been raised and solutions explained.



Figure 5.1 Virtual view of RLV prototype

5.2 Origins of the idea to build a vector rocket?

As explained in the introduction, the aim of making a model myself is to understand the real challenge of the RLV. Where does my idea come from? I do not know but I remember seeing the video of the Grasshopper of Space X and maybe the idea was born at this time. It was one pretty small rocket compared to the giant current size of Falcon 9 or Heavy. This prototype needed to pass a very simple test: to reach 1000 m high and come back to the takeoff/landing zone, simpler to say harder to realize. That will be another challenge for my thesis.



Figure 5.2 Space X prototype Grasshopper reach 1000m in June 2013

5.3 Characteristic of the model

The models need to follow this list of requirements:

- vector rocket
- cylinder shape
- autonomous stability
- controllable via remote control
- cameras to see the landing area

The presence of cameras on the requirements list is due to a parallel project, conducted by another student, where the goal is to improve the last stage of landing, at the touchdown moment. To be more accurate regarding the landing zone, we chose to use direct vision. Real-time information from the camera fixed to my model should have been able to provide some helpful support to develop the project.

To build successfully a rocket that takes into account all of these requirements, different models of RLV have been tentatively built, tested, improved as every industrial R&D project has to be. The work-in-progress steps have been detailed in the following section to end up by selecting the final RLV version. To compare and for a better understanding of each model, four key-points have been presented and summed up: evolution, new idea, flight, and disadvantages.

5.4 RLV Model 1

Even if this model stayed at the preliminary stage of a 3D model. Many ideas in conception have been used in the final version. The global shape is a cylinder according to the study's requirement. The general mechanism of the control engine is quite interesting and needs to be tested.

Evolution

This model is the first one, so the comparison will be with the standard RLV built by aerospace companies. Firstly, the engine will not be thermic but electric. Secondly the angle control of thrust will be directly controlled, because the engine is placed on the two centers of rotation. Due to using of a propeller's propulsion, it is necessary to use two engines to be able to control the yaw axis. The electric engine is lighter than the thermic one but the battery is heavier than fuel, as always argued. Except the size, global shape compared to standard RLV remains close.

New idea

The most interesting idea of this model is the mechanism of controlling engine which is inspired by the mechanism of gimbal in order to stabilize the camera [45,46]. Thus, the two-engines block is placed on the axis of the two rotations control pitch and roll.

The airflow has been taken into account on this model with several holes in the structure to ease air access to the propellers.

Flight

This model stayed a virtual 3 dimensions model.



Figure 5.3

Virtual view of RLV Model 1

Disadvantages

Major problem from the engine mechanism is that this model is not mountable. The next model has to take that into account.

5.5 RLV Model 2

RLV Model 2 is the first one physically built and the first one tested. Many problems have been solved thanks to this version, including control, power, structure, printing parameters. However, this model showed other problems that were impossible to solve without reviewing the entire model.

Evolution

This model is built with two different materials, with PLA plastic printing [31] for the engine legs and support engine, cardboard material for the pipe. The control engines keep the same idea as RLV Model 1 but this one is mountable (Annex 5.1). The detailed view explains the solution that has been developed.

New idea

Every part has been printed in PLA with the 3D printing process. The rotation of each engine axis is controlled by servos. The engines are 3 phases engines, the link between them and the flight controller is ensured by electronic speed control (ESC) [47]. The flight control (Matek Kakute F7 AIO controlled by INav) is used to control the flight. This model includes the development of the camera system, as explained on the 5.7.1

Flight

Several flight tests have been done (Annex 5.2). These tests aim to determine with accuracy the value of PID control. The value was found thanks to the model done on the chapter 4.

Disadvantages

The main problem of this model is weight. the RLV cannot fly because its mass was definitely too heavy. The next model has to be much lighter. Airflow was less efficient compared to Model 1.

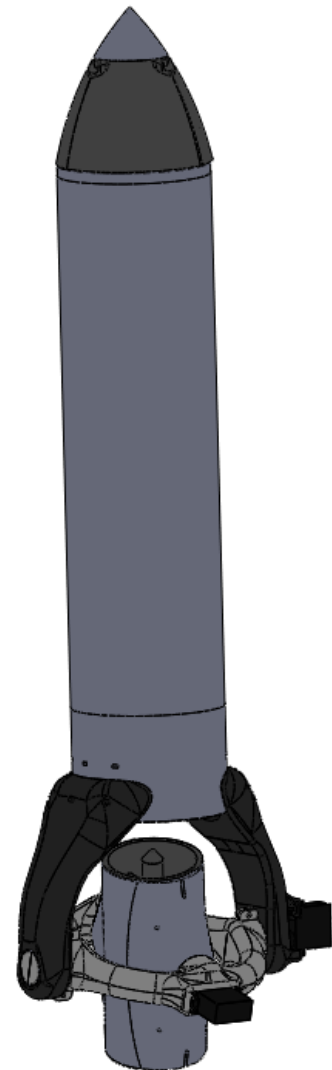


Figure 5.4

Virtual view of RLV Model 2

5.6 RLV Model 3

This model is the evolution of Model 2, the engines are the same, the servos are the same, the general shape is the same, however, the ratio power to mass is three times higher, each material has been reviewed, to get rid of unnecessary mass.

Evolution

The pipe is totally new, this new one will be 3D printed, it is two times lighter than the previous one and it takes already into account some support for the flight controller, battery and ESC. This shape gives a perfect airflow circulation to give more power to the engines.

The mechanism of control engine and legs are printed again with another shape of printing inside, to be lighter and still strong enough to support efforts.

New idea

Nothing new on the conception's side itself compared to the Model 2, but all equipment has been reviewed and improved.

Flight

Thanks to the huge weight reduction, the Model 3 had enough power to lift itself. However, one problem in the control of the yaw axis remained: the model was turning around itself.

Disadvantages

The problem to control the rotation around the yaw axis has to be solved to have a stable flight. Unfortunately, the problem comes from the ESC speed: they are not fast enough to compensate for the rotational forces.

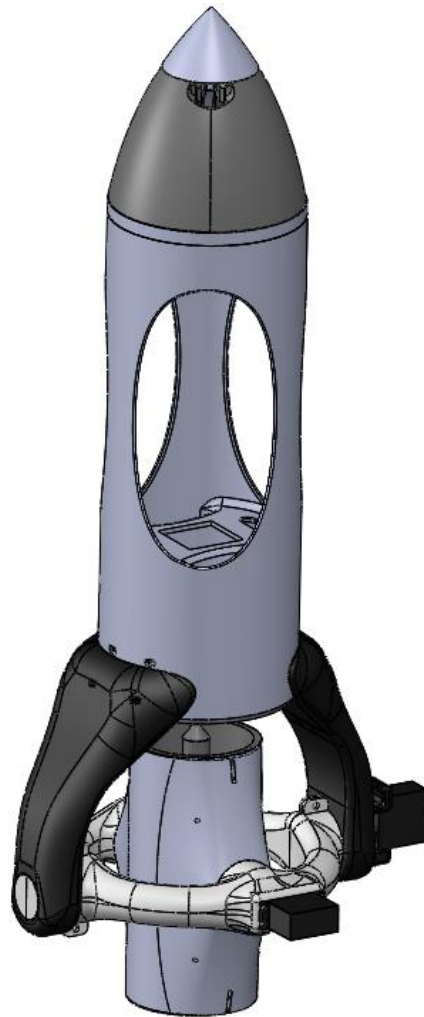


Figure 5.5

Virtual view of RLV Model 3.

5.7 RLV Model 4

This model is the good one, thanks to the experiences compiled from previous models. This model is smaller, the ratio of power to mass is two times hight than the Model 3.

Evolution

This model is smaller than Model 2 and 3, thus the engines, ESC, servo, and battery have been adjusted and scaled down. However, the mechanism of control engine is the same but revised to the new dimensions.

New Idea

To be sure that the engine will not give an uncontrollable yaw axis, the ESC selected has a better refresh rate. The engines are also new, and this kind of engines are developed to works on the same axis (Annex 5.4) To increase the position of the RLV, a GPS device is added. To increase the stability of the engine the battery is placed closer to the thrust center.

Flight

To control this model the value of PID has to be found precisely. The MATLAB Simulink model helps us by providing a rough value. To improve it, the only way was to make several tests. The flight is autonomously stable and controllable via a remote controller and via GPS coordinates.

Problem

This model had no camera. Unfortunately, given the weight constraint, cameras have been removed for which no reduction in weight was looking achievable.

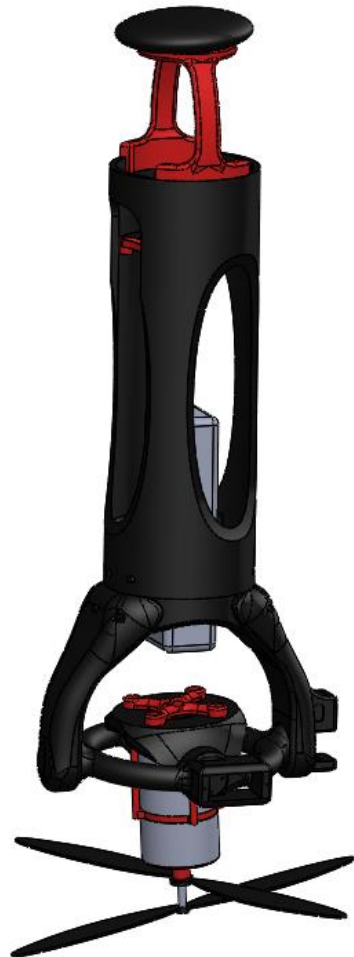


Figure 5.6

Virtual view of RLV Model 4

5.8 Analysis and remarks

This part has for aim to explain more about the previous ones. To built these models, some engineering and interesting challenges have been done. I chose to present two of them: firstly, I will present the process of construction of the structure, done via 3D printing. Secondly, I will develop the programming control who works in the model, by using a flight controller.

5.8.1 3D printing

3D printing is becoming an essential step in the creation of new mechanical parts. After the computer design and before the industrialization of the product. That gives to engineers the possibility to test and try the products. The rapidity of the creation and the facility to make parts give well advantage in process design. For my models the industrialization is not planned, however, the possibility to test the printed parts function of the others like engines and servo was very useful and at very low cost.

During the structure creation, the main evolution was between model 2 and model 3. Because after tests the model 2 was classified too heavy to be able to fly. Two solutions were possible; change the engines to be more powerful and keep the initial structure or keep the same engines with a new lighter structure. The second solution has been selected. Thus, the structure should evolve, it was a 3D printing challenge (Annexes 5.3, 5.4, 5.5).

5.8.2 Programming control

The control of our models is very close to the control of UAVs from a programming point of view, through the use of a flight controller made for aircraft or UAV. The sensors are multiple, accelerometer, gyroscope, barometer, magnetometer and GPS. A Kalman filter is used to filter the input data. The results are an acceleration of 3 ($\ddot{x}, \ddot{y}, \ddot{z}$) and an acceleration of 3 rotations ($\text{pitch}, \text{rôle}, \text{yaw}$). For the control, the programming is done via INAV; a software to program the flight controller. The complex settings are the PID coefficients, helped by equations 4.18, 4.19 and 4.20 found in chapter 4, a first value approach is determined. Through tests, these values are improved to give better stability to the model, this step of the process is done only for the model 5, the only one able to fly.

5.9 Special device developed

5.9.1 Vision system

To be able to control the landing accurately a vision system has been developed. This system has to support three cameras. They have to be fixed to the top of the structure to be able to perfectly overview the landing pad during the last step of the reentry. To decrease the drag force during the takeoff and increase during the landing a clever device has been modeled and printed in 3D in order to valid the conception.

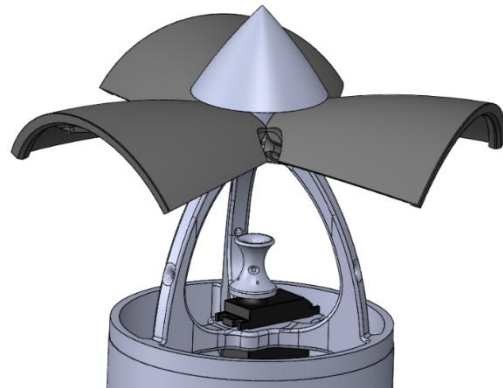


Figure 5.7 Solidworks view of vision system (top)

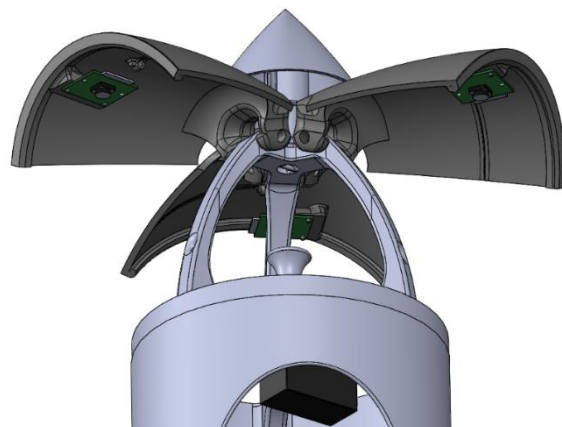


Figure 5.8 Solidworks view of vision system (bottom)



Figure 5.9 Photo of vison system printed in 3D

5.9.2 Support of Flight control system



Figure 5.10 Photo of the flight controller inside the RLV Model 2 pipe

5.10 Conclusion

Building these RLVs' models took me a long time, from 3D computer drawings and simulations to final realization and tests but it was interesting in many ways. Autonomous to conduct this project, it took me time to organize ideas, to progress step by step, and to get a result. My motivation helped me to overcome failures, even so, it is always hard to admit its own mistakes and doubts. At the second failure, with the Model 3, it was not easy to throw away all the work that was done previously and to be back to a blank page. However, I see there is a lot to learn as well from unsuccessful trials and, in my case, it was "almost" necessary to realize the next RLV version had to be smaller. This project was multi-disciplinary, that is why doing it by myself gives me a real experience in research and development.

Satisfaction was even greater when, after several months of work, the Model 4 succeeded to keep balance and was controllable.

Chapter 6 Conclusion

6.1 Summary

Our study was divided into four parts, the first one focused on the shape of the RLV. Then, the trajectory during the reentry phase was analyzed. Next, the stability of a vector rocket during the terminal phase of the reentry was modelized. In the last part of the project, the small electric rocket was built. Each of these parts has been reviewed, after in the way to always include improvements from my original thoughts.

The study of the shape of the RLV and the study of the atmospheric reentry trajectory need to be understood as a whole. For that purpose, the selected trajectory controller is the best to control attack angle of the RLV but not the best to add a direct drag force. The RLV's attack angle is key for drag effects. Thus, the air contact surface is not just the bottom of the RLV but potentially the whole structure. Furthermore, controlling this angle makes the rocket controllable in trajectory. The study of the trajectory shows that it makes it possible to improve the drag effects by rotating the RLV around a predefined trajectory.

The last two studies, the stabilization of a rocket vector and the construction of an electrical model, are also linked. The results of the modeling give some help for the determination of the PID corrector values of the RLV model. The construction of the model is an important part of the thesis. It gives the realization step that is sometimes missing in the aerospace projects.

6.2 Discussion and future works

With the widely use of RLV, its shape will certainly continue to be improved, especially if we think about ambitious projects of human transport, with the use of orbital speed that could become reality. Passengers' seats and comfort, size, or new energy sources may add new requirements and shape adjustments. However, one thing will remain the same: the shape of the RLV will depend on the path of the trajectory. For example, if a vertical landing is chosen, the RLV must have an additional air drag system. In case the trajectory could accept a high angle of attack, this improvement presented should provide some documentation to go one step further in the development of commercial projects.

For the stabilization of the vector rocket, even if the PID proves to be efficient, the next goal is to switch to AI control, at the pilot's propulsion axis. An AI control system is under development and the final goal is to control the high instability of the RLV.

For the small RLV model, a camera system adapted to make an automatic landing with vision control is to be built. The last objective is to improve the control of the model with the future developed AI.

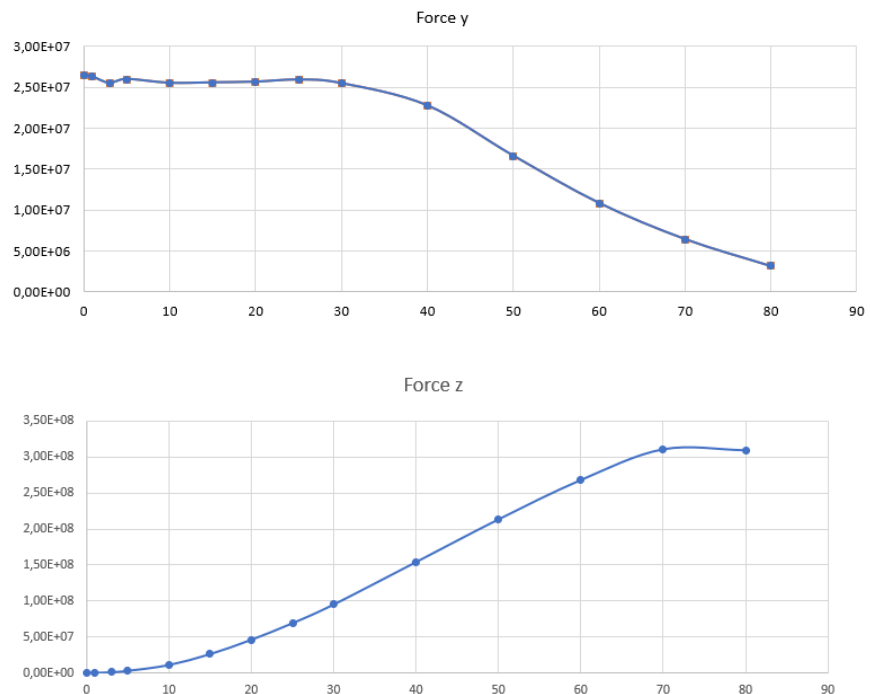
Bibliography

- [1] www.spacex.com/falcon9
- [2] www.spacex.com/falcon-heavy
- [3] The emerging orbital space tourism industry: new insight into demand and prospect for success, D. DePasquale, A. C. Charania, and J. R. Olds
- [4] www.spacex.com/starship
- [5] www.nasa.gov/mission_pages/shuttle/main/index.html
- [6] www.ariane.group/en/commercial-launch-services/ariane-5/
- [7] www.ariane.group/en/commercial-launch-services/ariane-6/
- [8] <https://cnes.fr/fr/callisto>
- [9] <https://cnes.fr/fr/search/site/themis>
- [10] www.isro.gov.in/launcher/rlv-td
- [11] <https://linkspace.com.cn/rlv.html>
- [12] www.blueorigin.com/new-shepard/
- [13] www.blueorigin.com/new-glenn/
- [14] www.blueorigin.com/blue-moon
- [15] Aerodynamic–structural missile fin optimization, Nenad Vidanovic
- [16] Multidisciplinary Design Optimization of Missile Configurations and Fin Planforms for Improved Performance D. Lesieutre, M. Dillenius, and T. Lesieutre
- [17] Design of a grid fin aerodynamic control device for transonic flight, Erdem Dikbas
- [18] Aerodynamics of projectiles with wrapped around and grid fins, Sher Afzal
- [19] Study of Swept Angle Effects on Grid Fins Aerodynamics Performance G A Fazal
- [20] Analysis of Grid Fins for Launch Abort Vehicle Using a Cartesian Euler Solver, James E. Kless and Michael J. Aftosmis
- [21] RLV Concept Employing Staged Rocket Engines, Robert Nelson
- [22] Different Approaches to Optimise Reusable Launch Vehicles Trajectories Christophe Talbot
- [23] Cavallo, A. and Ferrara, F., “Atmospheric Re-Entry Control for Low Lift/Drag Vehicles
- [24] A Reentry Trajectory Planning Based on the Optimization of Angle of Attack Yang Zhuo Zhang Qingzhen Tao Xiaoqiang

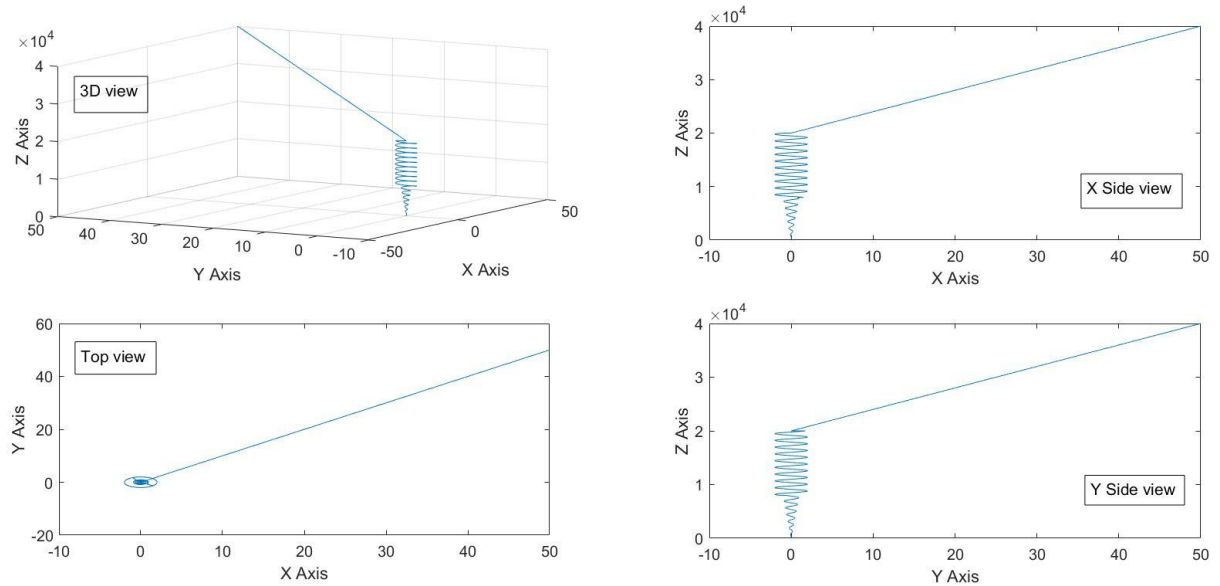
- [25] Chaturvedi N. A., Bacconi F, Sanyal A. K., Bernstein D., McClamroch N. H. "Stabilization of a 3D Rigid Pendulum"
- [26] The 3D Linear Inverted Pendulum Mode: A simple modeling for a biped walking pattern generation Shuuji Kajita, Fumio Kanehiro, Kenji Kando, Kazuhito Yokoi and Hirohisa Hirukawa
- [27] www.youtube.com/watch?v=RMeEh5OUaDs Ikarus electric "rocket" - Thrust-vectorized flying ducted fan tesla500
- [28] www.youtube.com/watch?v=AnGWM0yDfp0&t=42s Brushless R/C Rocket Vertical Landing with Pop Up Fins – RCTESTFLIGHT
- [29] www.spacex.com/news/2015/08/31/grid-fins
- [30] www.grc.nasa.gov/WWW/BGH/reynolds.html
- [31] http://www.adilca.com/INERTIAL_FORCE.pdf
- [32] www.grc.nasa.gov/www/k-12/airplane/dragsphere.html
- [33] khan academy – simple pendulum review
- [34] https://web.iit.edu/sites/web/files/departments/academic-affairs/academic-resource-center/pdfs/Moment_Inertia.pdf
- [35] A Summary of NASA Rotary Wing Research: Circa 2008–2018 Gloria K. Yamauchi, Editor Ames
- [36] <http://www.astronautix.com/r/roton.html>
- [37] Design of Optimal Attack-Angle for RLV Reentry Based on Quantum Particle Swarm Optimization Qing Zhen Zhang, Zhenbo Wang, Fei Tao
- [38] Atmospheric mass by altitude according to barometric levelling model. Marcel Délèze
- [39] www.mathworks.com/help/matlab/ref/polyfit.html
- [40] Transpiration Cooling Performance in LOX/Methane Liquid-Fuel Rocket Engines Andrea Bucchi
- [41] NASA Thermal Protection Materials and Systems: Past, Present, and Future, Sylvia M. Johnson
- [42] www.mathworks.com/help/sl3d/vrsink.html
- [43] <https://fr.mathworks.com/discovery/pid-control.html>
- [44] www.space.com/spacex-starhopper-aces-final-test-launch-landing.html
- [45] Data-Driven PD Gimbal Control, KazuoKawada
- [46] A control system for a 3-axis camera stabilizer, Ali Algoz Bakhtiyar Asef Hasnain
- [47] www.modelflight.com.au/blog/electronic-speed-controllers

Annexe

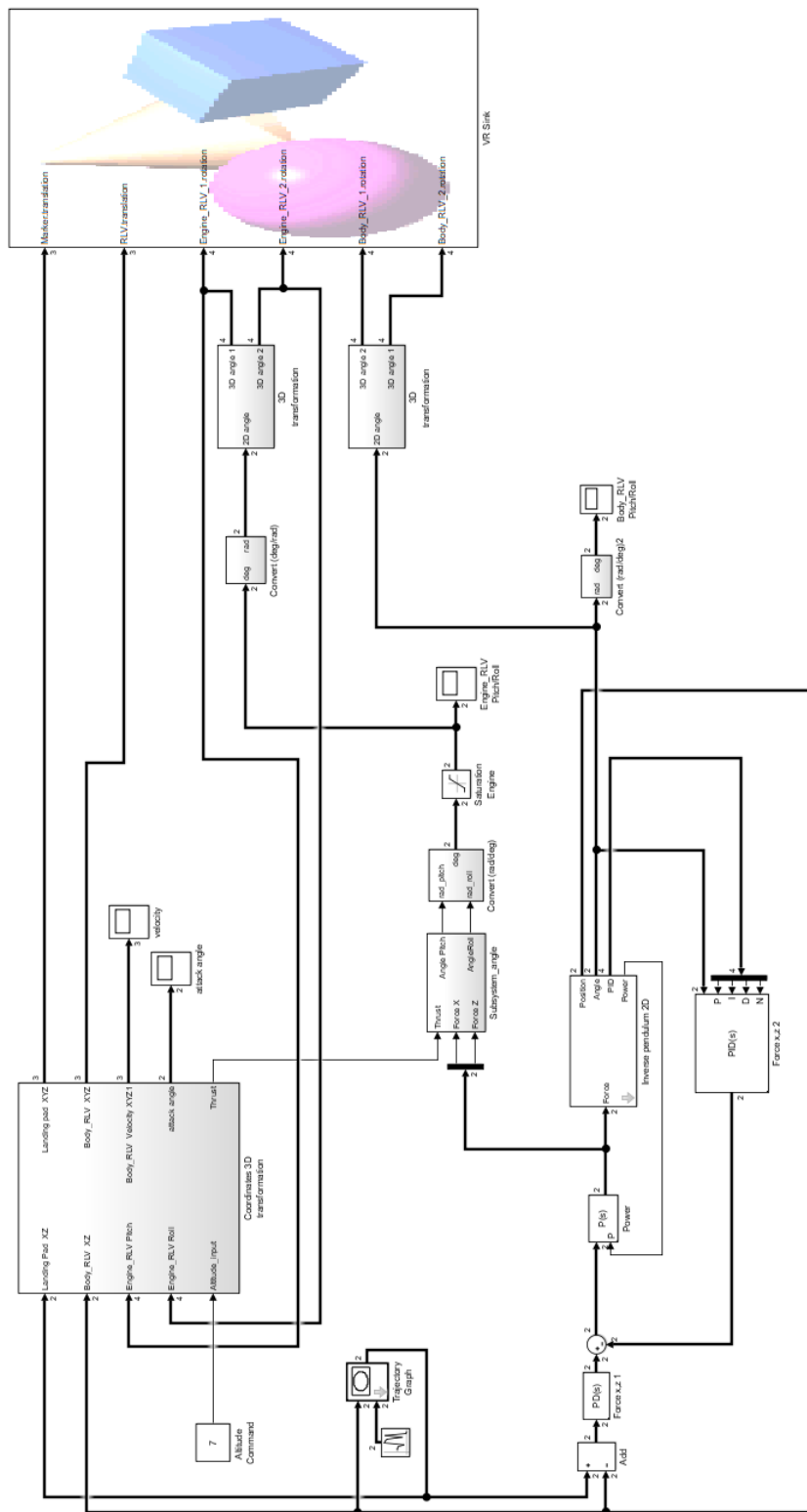
Annex 3.1: Force Y and Force Z function of attack angle:



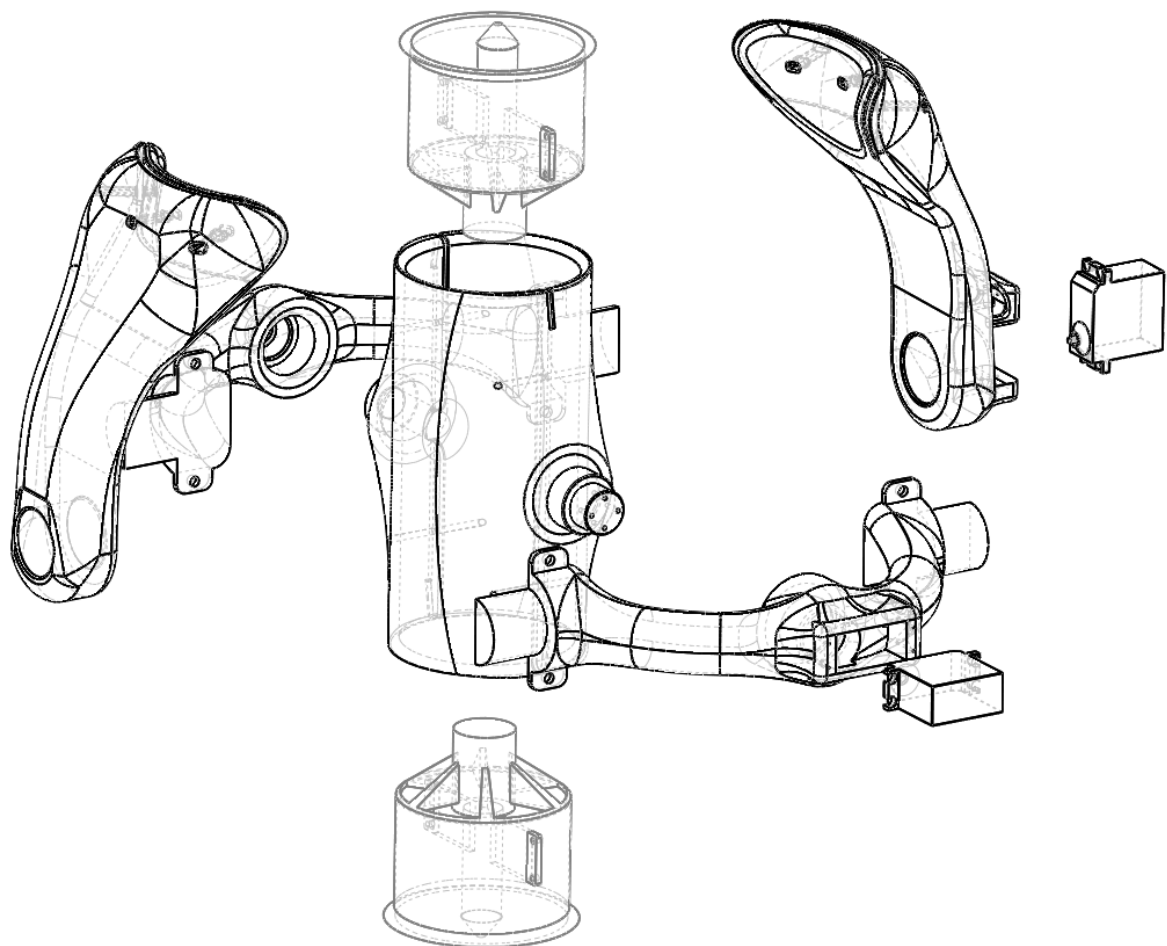
Annex 3.2: All views of top RLV trajectory:



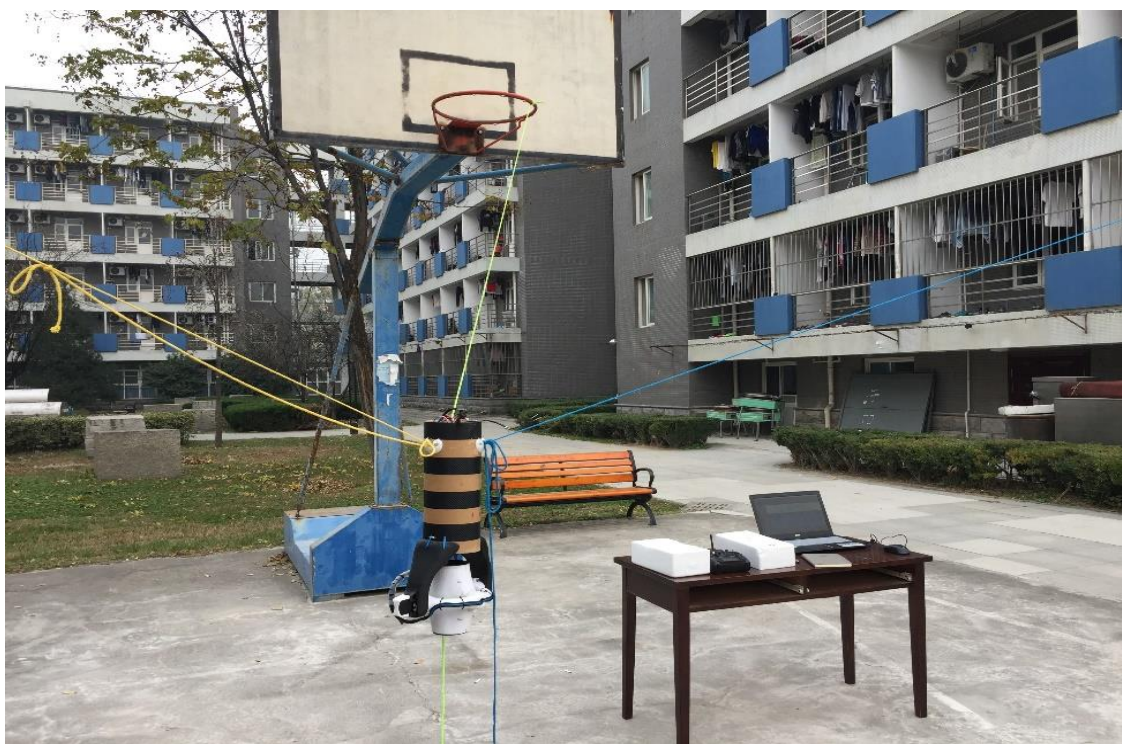
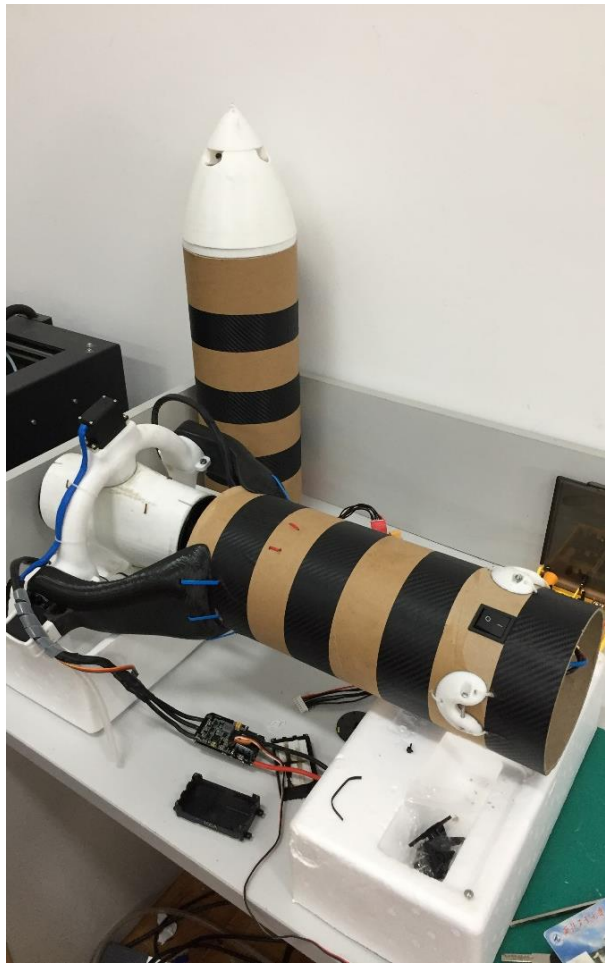
Annex 4.1: Full Simulink model of vector rocket control:



Annex 5.1: Exploded view of mechanism of control engine:



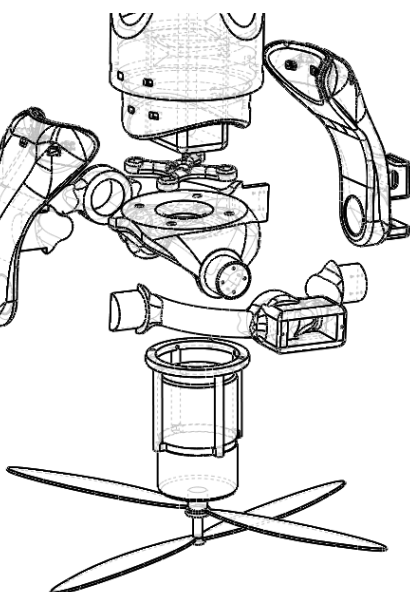
Annex 5.2: Real RLV Model 2:



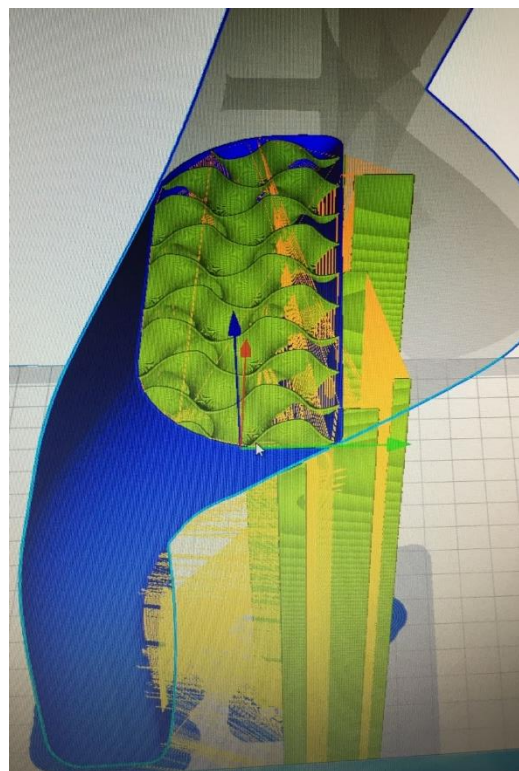
Annexe 5.3: Real RLV Model 3:



Annexe 5.4: Real RLV Model 4:



Annexe 5.5: Printed structure:



西北工业大学

学位论文知识产权声明书

本人完全了解学校有关保护知识产权的规定，即：研究生在校攻读学位期间论文工作的知识产权单位属于西北工业大学。学校有权保留并向国家有关部门或机构送交论文的复印件和电子版。本人允许论文被查阅和借阅。学校可以将本学位论文的全部或部分内容编入有关数据库进行检索，可以采用影印、缩印或扫描等复制手段保存和汇编本学位论文。同时本人保证，毕业后结合学位论文研究课题再撰写的文章一律注明作者单位为西北工业大学。

保密论文待解密后适用本声明。

学位论文作者签名: _____ 指导教师签名: _____

年 月 日

年 月 日

西北工业大学

学位论文原创性声明

秉承学校严谨的学风和优良的科学道德，本人郑重声明：所呈交的学位论文，是本人在导师的指导下进行研究工作所取得的成果。尽我所知，除文中已经注明引用的内容和致谢的地方外，本论文不包含任何其他个人或集体已经公开发表或撰写过的研究成果，不包含本人或其他已申请学位或其他用途使用过的成果。对本文的研究做出重要贡献的个人和集体，均已在文中以明确方式表明。

本人学位论文与资料若有不实，愿意承担一切相关的法律责任。

学位论文作者签名: _____

年 月 日